U.PORTO

FEUP FACULDADE DE ENGENHARIA UNIVERSIDADE DO PORTO

MASTER IN ENVIRONMENTAL ENGINEERING 2022/2023

ESTABLISHMENT OF A LABORATORY SCALE TEST RIG FOR ELECTROCHEMICAL LIGNIN CONVERSION

FRANCISCO NUNES PEREIRA

Dissertation submitted for the degree of

MASTER IN ENVIRONMENTAL ENGINEERING

President of the jury:
Adrián Manuel Tavares da Silva, Associate Professor, Department of Chemical Engineering, Faculty of Engineering, University of Porto

_____

Supervisor at the University:
Prof. Dr. M. Fernando R. Pereira, Department of Chemical Engineering, Faculty of Engineering, University of Porto

_____

Supervisor at Foreigner University (or at Company):
Roman Tschentscher, Senior Scientist, Process Technology, SINTEF Industry

_____

February, 2023

Acknowledgments

This thesis work and this internship were very challenging, probably the most stimulating 5 months of my academic journey. Being in a foreign country, not speaking in my native language, learning a new culture and getting used to the Norwegian weather were not simple tasks but they got a little easier with all the support that was given to me.

I would like to thank every person I came across in SINTEF, for the hospitality and sympathy, but I have to specially thank Roman Tschentscher, my supervisor from SINTEF, for his tireless and unconditional support. All the knowledge you shared with me was crucial for this work. I would just like to say that it was a pleasure to work and learn with you.
I also want to thank my Academic Supervisor, Professor Fernando Pereira, for accepting this challenge and for guiding me in the right direction.

My family, the main support of my life, deserves the greatest thanks, for giving me the strength and confidence that I need to keep doing my best in everything I do. Thanks for you believing and investing in me!

I also need to mention my friends that were by my side on this journey. My friends from school, university and, more recently, from SINTEF. Thank you all for being part of my life and for all the happy moments and positive energy.

To Carina Sá, my girlfriend, for being with me since day one and for her precious advice, even though I didn't always follow them. Thanks for all the patience, kindness, and companionship!

To conclude, I want to thank everyone and the ones I may have forgotten and not stated here. I am very proud of myself but also aware that it would have been much more difficult without all of you.

Big thanks to each one of you!
As one of my favourite artists says, "Nobody is running more than us" Força Suprema.

Abstract

Kraft lignin dissolved in black liquor is a high potential feedstock for phenolic platform chemicals and biofuels. Currently, this black liquor fraction is densified and burnt for energy generation purposes in recovery boilers. Depolymerising parts of that fraction while dissolved in black liquor without affecting the kraft pulping process would create an additional value chain for pulp mills.

This work focuses on the electrochemical conversion of kraft lignin dissolved in black liquor. Such a process operates at mild conditions and can, in principle, be integrated into the evaporation train of the liquor cycle. Most importantly, it does not require any alteration of the black liquor. In this project, a lab scale test rig was established and tested for industrial black liquor conversion by varying several process parameters. The setup enables to run batch and continuous electrochemical conversion processes semiautomatically with high reproducibility.

The electrochemical lignin conversion experiments were carried out in a batch system, using an electrochemical flow through a cell designed at SINTEF. Three combinations of electrodes were applied. Nickel was used as the anode material in all combinations. The cathodes tested were nickel, copper and stainless steel. Two types of electrochemical tests were performed: chronoamperometry tests to identify the stable operational window and constant voltage tests to assess the electrode stability. In addition to recording the current, the production of hydrogen and oxygen was monitored online using gas chromatography, respectively. During constant current stability tests, black liquor samples were taken periodically for further analysis using gas chromatography, nuclear magnetic resonance and gel permeation chromatography. The data show clearly that lignin condensation is the dominant process when applying intermediate black liquor. Monomeric phenolics are consumed and lignins are formed, which have a higher molecular weight than the feedstock lignin. Recommendations for process improvement and understanding of the reaction mechanisms are given.

Keywords (theme): Black Liquor / kraft Lignin / Electrochemical Conversion / Nickel Electrode / Stainless Steel Electrode / Copper Electrode / Chronoamperometry / Chromatography

Resumo

A lignina Kraft dissolvida em licor negro é uma matéria-prima de alto potencial para produtos químicos fenólicos e biocombustíveis. Atualmente, esta fração de licor negro é densificada e queimada para fins de geração de energia em caldeiras de recuperação. A dissoluções das partes despolimerizadas no processo kraft do licor negro sem afetar o processo, faz com que possa ser desenvolvido um processo com valor adicional para a indústria da celulose. Este trabalho concentra-se na conversão eletroquímica da lenhina kraft dissolvida em licor negro. O processo opera às condições industriais e pode, em princípio, ser integrado na cadeia processual de evaporação do licor negro. Neste projeto, foi estabelecido e testado um equipamento de teste à escala laboratorial para a conversão industrial do licor negro, através da variação de vários parâmetros processuais. A configuração permite executar processos de conversão eletroquímica contínua e descontínua, de forma semiautomática. As experiências de conversão eletroquímica de lignina foram realizadas num sistema batch, utilizando uma célula eletroquímica, a qual foi concebida no SINTEF. Três combinações de elétrodos foram testados, níquel foi utilizado como material anódico em todas as combinações. Os cátodos testados foram, níquel, cobre e aço inoxidável. Foram realizados dois tipos de testes eletroquímicos: Testes de cronoamperometria, para identificar a janela operacional estável e testes de voltagem constante para avaliar a estabilidade dos elétrodos. Para além do registo da corrente, a produção de hidrogénio e oxigénio também foi monitorizada recorrendo à cromatografia gasosa. Durante os testes de estabilidade de corrente constante, foram recolhidas periodicamente amostras de licor negro para análise posterior, utilizando a cromatografia gasosa, a ressonância magnética nuclear e a cromatografia de permeação de gel. Os dados mostram claramente que a condensação de lignina é o processo dominante quando se aplica licor negro intermédio. São consumidos fenóis monoméricos e formam-se ligninas, que têm um peso molecular mais elevado do que a lignina que é alimentada sob forma de licor negro. No final foram tecidas algumas recomendações para a melhoria do processo e compreensão dos mecanismos de reação.

Palavras-Chave (tema): Licor negro / Lignina Kraft / Conversão Eletroquímica / Níquel elétrodo/ Aço Inoxidável elétrodo / Cobre elétrodo / Cronoamperometria / Cromatografia

Index

List of Figures

List of Tables

Notation and Glossary

A	Area	m^2
AH_2 *or* AH_2	Current	A
C	Concentration	% (mol/mol)
N	Molar number	mol
$\dot{n}$	Molar Flow	mol/s
P	Pressure	Pa
R	Ideal Gas Constant	$m^{-3}\ Pa\ K^{-1}\ mol^{-1}$
S	Selectivity	%
T	Temperature	ºC
V	Volume	m^3
$\dot{V}$	Volumetric Flow	m^3/s

List of Acronyms

BL	Black Liquor
EC	Electrochemical Cell
HPLC	High Performance Liquid Chromatography
NMR	Nuclear Magnetic Resonance
GC	Gas Chromatography
GC-MS	Gas Chromatography – Mass Spectrometry
GPC	Gel Permeation Chromatography
SS	Stainless Steel
SEC	Size Exclusive Chromatography
STP	Standard Temperature and Pressure
RID	Refractive Index Detector

1 Introduction

1.1 Context and thesis objective

The preoccupation and conscience with the Global Climate Change and Global Warming phenomenon are growing. Efforts to decrease the need for fossil fuel usage are evident. Renewable energies are being explored, implemented industrially, and growing over time. Wind power, solar power, and energy from biomass like biogas supply around 14 % of the total world energy demand.

In this perspective, the valorisation of technical lignins, which represent one side-stream of the existing industrial-scale biorefineries and paper industry, is a strategic approach to enhance the biorefinery and paper industry sustainability and provide biobased platform chemicals to the transport energy and chemical sectors. Lignin is an abundant biopolymer and the dominant direct source of functionalised aromatic compounds. The production of lignin-based phenolics at the pulping site would be a valuable add-on to the pulping industry to diversify its product portfolio and increase economic stability, including job security in rural areas. Such a process needs to comply with the pulping conditions to minimise changes and modifications of the pulping steps.

In this work, we explore the electrochemical oxidation of lignin, as a part of the H2020-project EBIO. With the aim of producing monomeric phenolics, the operational window is evaluated with respect to various process parameters and recommendations are given for further optimisation. The work forms a solid basis for scale-up studies.

1.2 Presentation of Institute

Today's SINTEF is one of the biggest independent research institutes in Europe, established in 1993 by merging the Oslo-based Sentralinstitutt for industriell forskning and the Trondheim-based SINTEF. It is a non-profit organisation that includes more than 2 000 employees coming from 75 different nationalities. The organization is divided into six institutes: Community, Digital, Energy Research, Industry, Manufacturing and Ocean. The work was carried out in the institute SINTEF Industry, within the department of Process Technology. This department has a strong focus on chemical conversion and separation processes operating in the domains of homogeneous and heterogeneous catalysis, and gas

capture at a lab to pilot scale. Supporting services include flow sheeting, and feasibility analyses in cooperation with other departments.

1.3 Contribution of the Author to the Work

In the first part of my thesis work, I executed experimental experiments to get familiar with the electrochemical cell, in terms of its constituent elements and the respective experimental setup. After this phase, I optimised the electrode design, where I redesigned each electrode to avoid liquid leaks during the experiments. Later, the gas phase was calibrated with three reference gas bottles. Thus, it was possible to optimise the online gas product analysis during the electrochemical reaction.

After ensuring the stability and security of the experimental setup, I tested the influence of the experimental conditions. After understanding their influence, I performed two types of experiments: the chronoamperometry step test and the constant voltage stability test. In both tests, the gas phase products were analysed and studied using gas chromatography analysis. Black liquor samples were collected during the constant voltage experiments to be subsequently analysed by bio-liquid experts.

In the last few weeks, I performed tests where I modified the feedstock during the experiment and the black liquor composition, to include the influence of some parameters. Conclusions for process optimization, comprehension of reaction processes, and future scale-up were reached with the assistance of my SINTEF adviser.

1.4 Organisation of the Thesis

This report is organized into 6 different sections:

- **Chapter 2 – State of Art**

  Literature on the components of lignocellulosic biomass is included in the first portion of this article, with a specific emphasis on the lignin polymer and mentions of its structure, chemical makeup, and uses. To fully comprehend the makeup of the black liquor utilised as feedstock in the present industrial kraft lignin valorisation, the Kraft process will be reviewed. The outline of the thesis is also presented, explaining the electrochemical process developed for lignin electrochemical depolymerisation.

- **Chapter 3 – Materials and Methods**

  Here, the material and methods used in the experimental electrochemical lignin depolymerisation are demonstrated. Starting with the black liquor as feedstock,

explaining the electrodes and electrochemical cell selection, design and configuration. The Lignin Electrochemical Depolymerisation experimental setup is fully described together with the procedures used to perform both types of experiments, including the experimental conditions for each one. The calibration methods adopted for the analysis of the gas and liquid phase products are explained in detail and demonstrated.

- **Chapter 4 – Results and Discussion**

In this chapter, results obtained from the performed experiments are presented in tables and figures, followed by a discussion and analysis. The chapter is divided into five main parts: effect of experimental conditions, chronoamperometry step test, constant voltage stability test, product analysis and additional experiments.

- **Chapter 5 - Conclusion and recommendations**

In chapter 5, the conclusions reached during the work are stated. The most relevant results are mentioned and commented.

- **Chapter 6 – Assessment of the work**

A final appreciation about the project is presented.

2 State of Art

2.1 Raw Material - Wood

The composition and versatile properties of wood make it one of the most valuable renewable resources on the planet, used in different applications such as pulp production, structural timber, furniture, panels and the production of many composites [2]. As a major lignocellulosic resource, wood is defined as the interior tissue of perennial plant stems, branches, and roots. It serves vital functions for plants such as mechanical stability, water and mineral transport, and material storage [2]. Woody plants are organised into two botanical classes, softwoods (gymnosperms) and hardwoods (angiosperms) [20]. The average percentage, on a dry weight basis, of the structural polymers present in the plant cell wall, in all different types of nonedible biomass, is cellulose (40–50 wt %), hemicellulose (25–30 wt %) and lignin (15–20 wt %), illustrated in Figure 1 [16]. Table 1 summarizes the chemical composition with a particular focus on species of lignocellulosic biomass typically used by the pulp industry.

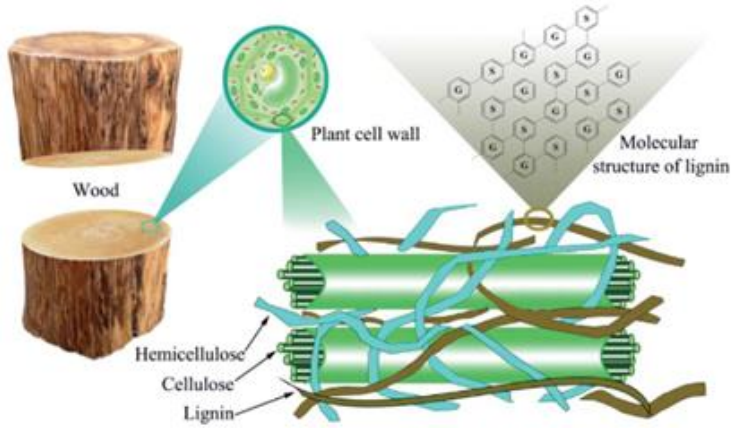

Figure 1 - Lignocellulosic biomass structure, with a focus on lignin structure. Adapted from: Penghui Li et al. [16].

In addition to the three main fractions, biomass contains a small percentage of other compound groups, including organic solvents (ethanol, acetone, dichloromethane, and benzene) [18]. Extractives are a diverse group of components that include waxes, fatty acids, gums, resins, chlorophyll, terpenoids, and different phenolic substances. They serve as metabolic intermediates, energy storage or defence mechanisms against microbial

attack. They also provide properties, such as colour, aroma and wilting resistance [18]. Another component fraction present in biomass are salts, composed of several inorganic compounds (i.e. calcium (Ca), potassium (K), magnesium (Mg) and silicon (Si) [18]. The exact wood composition is dependent on various factors, including location, season, type of biomass, tree section and plant age. Young wood contains fewer amounts of cellulose, hemicellulose and lignin than older woods [17, 18]. To extract specific components and fractions from lignocellulosic biomass including cellulose, hemicellulose, lignin, protein, and oil, several processing steps are required. [26].

Table 1 - Chemical composition (% Dry weight) of different Lignocellulosic Biomass Types. Adapted from: Solange I. Mussatto et al. [18].

General Biomass Classification	Lignocellulosic Biomass Type	Cellulose	Hemicellulose	Lignin
Hardwood	*American sycamore*	37.2-41.8	17.6-19.6	25.0-27.3
	Black Locust	3.3-42.6	16.6-18.9	24.4-28.6
	Eucalyptus	46.6-50.3	12.7-18.9	26.9-28.2
	Hybrid poplar	40.3-47.3	16.7-22.6	15.5-16.3
	Willow	42.4-45.3	20.6-22.9	16.9-18.9
	Oak	40.4	35.9	24.1
Softwood	*Pine*	42.0-50.0	24.0-27.0	20.0
	Spruce	45.5	22.9	27.9

2.2 Cellulose

Cellulose is the most abundant biopolymer on earth. It is a linear homopolymer of glucose ($C_6H_{12}O_6$) units linked together through β -(1.4)-glycosidic bonds, represented by its monomeric unit $(C_6H_4O_4)_n$ [18]. The small repetitive unit of cellulose is the dimer cellobiose, as highlighted in Figure 2. Cellulose fibres are insoluble in most conventional solvents, including water. The microfibrils of ≅ 3 nm in higher plants consist of well-packed, long hydrogen-bonded stretches of crystalline cellulose and less ordered amorphous regions, representing the main component of the cell wall in plants [20, 23].

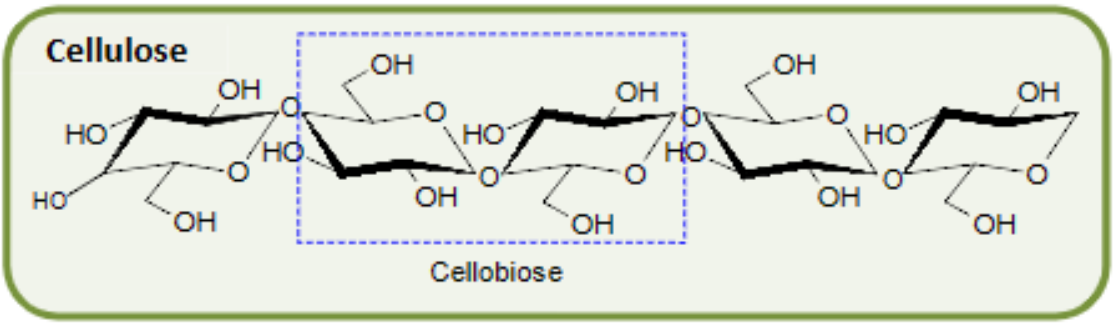

Figure 2 - Cellulose polymer structure. Adapted from: Solange I. Mussatto et al. [18].

2.3 Hemicellulose

Hemicellulose is the third most abundant component of lignocellulosic biomass. It is constituted by a heterogeneous group of matrix polymers of low molecular weight. The hemicellulose matrix is formed by pentoses (*D*-xylose, *D*-arabinose), hexoses (*D*mannose, *D*-glucose, *D*-galactose) and sugar acids, illustrated in Figure 3 [18]. Hemicelluloses constitute matrix polysaccharides together with pectin in primary cell walls, while for secondary cell walls, they are matrix polymers with lignin. They are connected to the surface of the cellulose microfibrils and between each other by hydrogen bonds. Hemicelluloses contribute to the strengthening of the cell wall by interacting with cellulose and lignin [18].

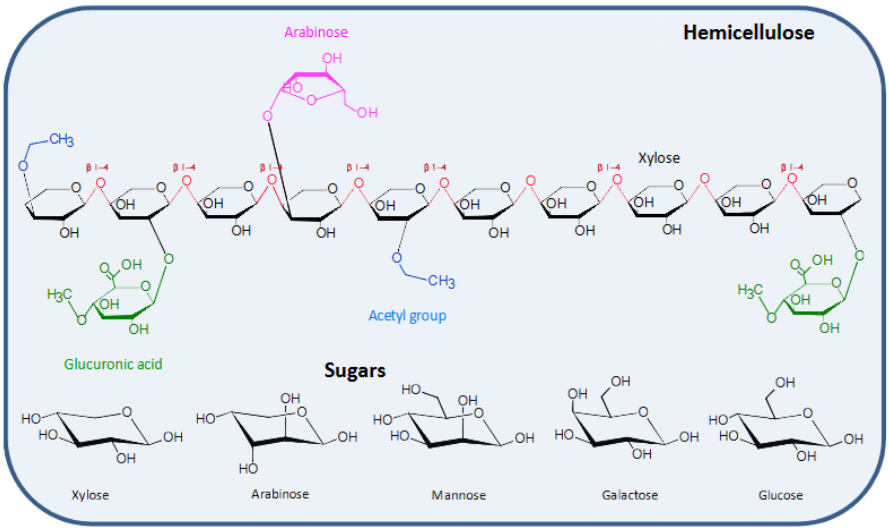

Figure 3 - Matrix polymers of hemicellulose. Adapted from: Solange I. Mussatto et al. [18].

2.4 Lignin

Lignin accounts for approximately 30 % of the organic carbon in the biosphere, and it is the second most abundant biopolymer present in lignocellulosic biomass [8]. Lignin fills the space between cellulose and hemicellulose supporting the matrix and the fibrils, represented in Figure 4.

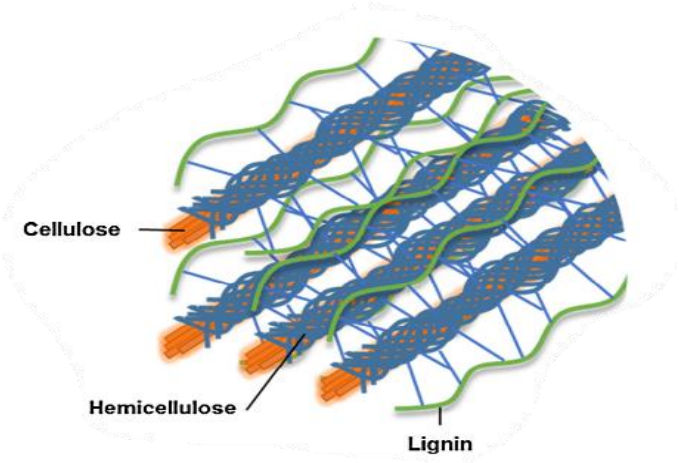

Figure 4 - Lignin Distribution in lignocellulosic biomass. Adapted from: Figueiredo Patricia et al. [8].

Lignin has an irregular and heterogeneous structure that provides rigidity and physical strength to the cell wall of biomass by acting as a binding material between cells that gives significant resistance to impact, compression, bending, and microbial attack [18], comparable to phenolic resins in wood composites. As lignin is the focus of this thesis, in the following section, lignin biosynthesis, structure and chemical composition, properties and technologies to isolate lignin will be reviewed.

2.4.1 Lignin Structure, Chemical Composition and Applications

The word lignin derivates from the Latin word “lignum”, which means wood [26]. Lignin does not have a constitutional definition, due to its complexity, but can be simplified as a class of phenolic natural polymers with a broad composition and a variety of linkages between the building units [9].

Lignin is synthesised by the cell at the end of its growth phase. The biosynthesis includes the radical polymerization of three main phenylpropanoid monomers (monolignols), namely p-coumaryl, coniferyl and sinapyl alcohol, represented in

Figure 5. The monolignols are synthesised in the cytoplasm and transported to the cell wall where the lignification occurs, specifically their integration as guaiacyl (G), syringyl (S), and p-hydroxyphenyl (H) units. Less common monomers are modified forms of hydroxycinnamyl alcohol, also shown in Figure 5. Lignin from softwood presents more guaiacyl (G) residues, lignin from hardwood contains a mixture of guaiacyl (G) and syringyl (S) residues, lignin from grass bears has an equal mixture of all three aromatic residues (G), (S) and (H). The most important functional groups in the lignin structure are methoxyl, hydroxyl, carboxyl and carbonyl groups, highlighted in Figure 6.

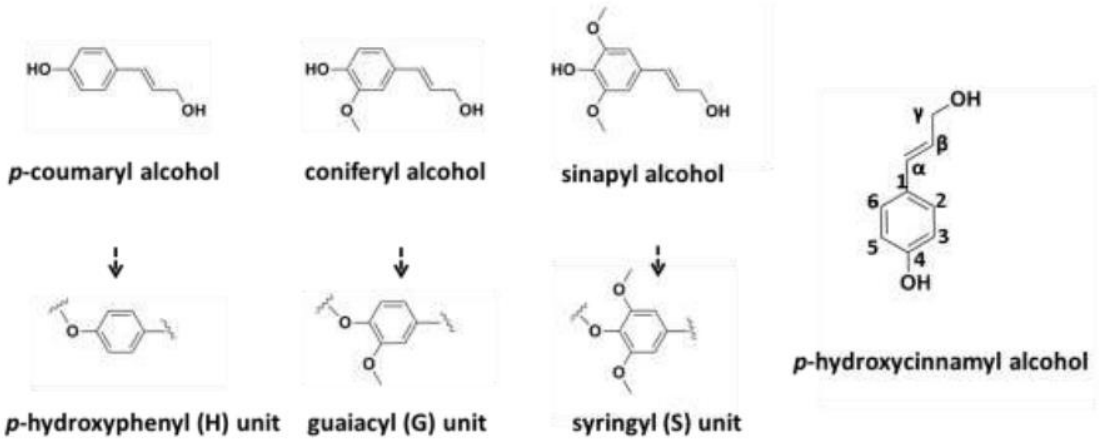

Figure 5 – Three principal lignin-building blocks, monolignols, above, the corresponding units found in the lignin structure, p-hydroxyphenyl (H), guaiacyl (G) and syringyl (S) units. On the right side is a p-hydroxycinnamyl alcohol structure with numbered carbon atoms. Adapted From: Dobado José, G. Calvo Flores Francisco et al. [9].

The complexity of the lignin structure is related not only to the different compositions and ratios of monomers but also to the many possible linkages between them. The different linkages can be split into eight categories:

- **Carbon-Carbon Bonds:** β -β, β -1′, 5-5′;
- **Carbon-Oxygen Bonds**: β-O-4′, α-O-4′ and 4-O-5′;
- **Carbon-Carbon and Carbon-Oxygen bonds:** β -5′/ α-O-4′, β- β′/ α-O-γ′;

The ether β-O-4 linkage is the most predominant, with 60 % of the total bonds present in the polymer. The linkages between the units give rise to the formation of substructures, among which phenylcoumarans (β-5) and resinols (β-β) are the most abundant.

The Lignin structure directly depends on the biomass type and is often referred to as softwood lignin, hardwood lignin or even grass lignin. The chemical composition approach, based on the biomass source is robust. Still, the lignin structures currently available in the

literature are only simplified models aiming to describe the yet unknown pristine form of the polymer. Further, this classification needs to be extended once we refer to technical lignins since lignin fractionation and isolation significantly impacts the chemical structure.

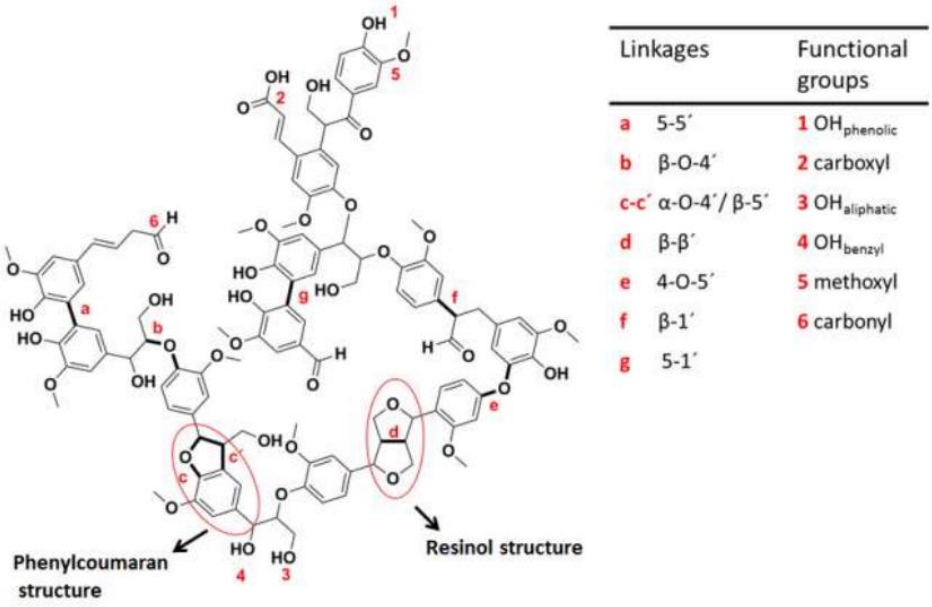

Linkages	Functional groups
a 5-5´	1 $OH_{phenolic}$
b β-O-4´	2 carboxyl
c-c´ α-O-4´/ β-5´	3 $OH_{aliphatic}$
d β-β´	4 OH_{benzyl}
e 4-O-5´	5 methoxyl
f β-1´	6 carbonyl
g 5-1´	

Figure 6 – Lignin Structure with the main functional groups, linkages and substructures. Adapted From: Dobado José, G. Calvo Flores Francisco et al. [9].

Based on their chemical structure technical lignins have specific properties defining their current and potential applications, which are listed in Table 2 [8].

Table 2 – General Lignin Properties and Applications.

Properties	Applications
Absorbs UV radiation	Protective, light harvesting paint/coating
Antimicrobial activity	Protective coating
Antioxidative properties	Applications in cosmetics
Biodegradable, CO_2 neutral	Bio-based alternative to resins, asphalts
High phenolics content	Functionalised phenols, solvents, resins

Lignins have good rheological characteristics, viscoelastic properties, film-forming capacity, and compatibility with a wide range of chemicals making them suitable for coatings, paints, etc. Still, a direct replacement of fossil-based phenols requires the adaption of the manufacturing process. Industrially two directions are explored, being one

the development of lignin-based process and products and the other the modification of the lignin properties to comply with established manufacturing processes.

2.5 Industrial fractionation of lignocellulosic biomass

The global paper and cardboard production in 2018 was approximately 420 million metric tonnes [25]. Based on this, it has been estimated that more than 70 million tonnes of industrial lignin are extracted from pulping processes around the world annually. The following chapters will give an overview of different techniques to extract lignin from lignocellulosic biomass, before focusing on kraft pulping as the dominant wood pulping process, according to Figure 7.

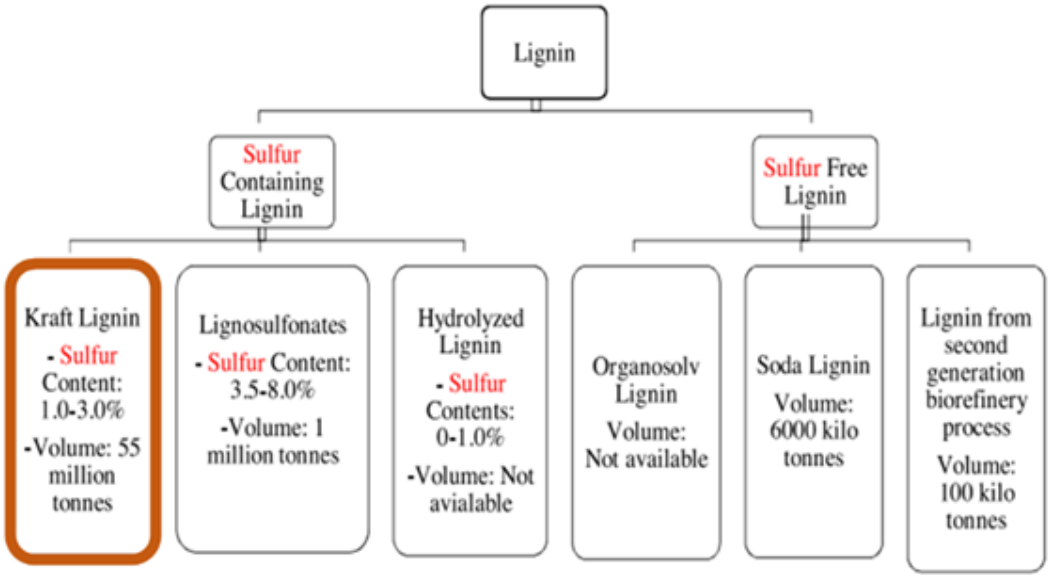

Figure 7 - Lignin sources and world annual volumes, 2019. Adapted from: D.S. Bajwa et.al [4].

Biomass pre-treatments are classified as physical, chemical, solvent fractionation and biological processes [18].

The focus of this section is on the chemical and solvent isolation processes of lignin, the other two classification categories will be not discussed as they are not relevant to the process. In the context of “lignin first” technologies, targeting lignin removal, the pre-treatment of lignocellulose aims to cleave the covalent bonds between lignin and the carbohydrate fraction [20].

The lignin source and the lignin extraction methodologies affect the obtained lignin composition and can lead to the parallel removal of other fractions. The process parameters are temperature, pH and pressure of the system, residence time, and the

capacity of the solvent/solute [8]. The various lignin extraction processes can be divided in terms of chemical and solvent techniques. Chemical treatments include the following processes: lignosulfonate process (sulfite process), kraft process and soda and alkaline processes and significantly alter not only the molecular weight distribution by depolymerisation and repolymerisation but also the chemical structure by oxidation and the introduction of sulfur groups, etc. Milder extraction technologies, such as ionic liquid and Organosolv technologies, retain the natural lignin structure but also significantly reduce the molecular weight. The technical lignin obtained after those processes are classified based on their extraction process as kraft lignin, soda lignin, alkaline lignin, lignosulphonates lignin, and organosolv lignin, etc., often but not always also providing the feedstock type. Table 3 shows a resume of treatment conditions and some chemical characteristics of technical lignins.

This thesis will focus on electrochemically converting black liquor (BL), produced by the kraft extraction process. The next section will discuss in detail the kraft process, to understand the chemical composition of BL and the chemical and physical characteristics of the dissolved lignin.

Table 3 - Characterization of Chemical and organosolv pre-treatments for lignin extraction. Adapted from: Figueiredo, Patrícia et al. [8].

Extraction process	Treatment Conditions	Solubility	Lignin MW (Da)	Functional Groups (%)		
				COOH	OH phenolic	Methoxy
Kraft Process	1st: Sodium hydroxide and/or sodium sulfide (pH = 13-14 and $T\pm$ 170 °C) → Kraft Lignin present in BL 2nd: Sulfuric acid (pH = 5-7.5)	Alkali and organic solvents	1000 -15000	4.1 [b]	2.6 [b]	1.4 [b]
Sulfite Process	Metal sulfite + Sulfur dioxide (Ca^{2+}, Mg^{2+} *or* Na^{+}), pH = 2-12 and T =120 -180 °C, for 1-5 h	Water	1000 - 50000	---	---	---
Soda and Alkaline	13-16 wt% of Sodium hydroxide (T=140 -170 °C) + Anthraquinone (catalyzer)	Alkali	1000 - 3000	7.2 - 13.6	2.5 - 5.1	10 - 16
Organosolv	13-16 wt% of Sodium hydroxide (T=140-170 °C) + Anthraquinone (catalyzer)	Wide range of solvents	500 -5000	3.6 - 7.7	3.4 - 3.7	15.1 -19

[b] *Values referred to softwoods*

2.5.1 Kraft Process

This is the dominant industrial process used in the pulp and paper industry [27]. The high strength of kraft pulp and the ability of the process to handle almost all species of softwood and hardwood, and the favourable economics due to high chemical recovery efficiency (about 97 %) give the kraft process an advantage over other pulping processes [27].

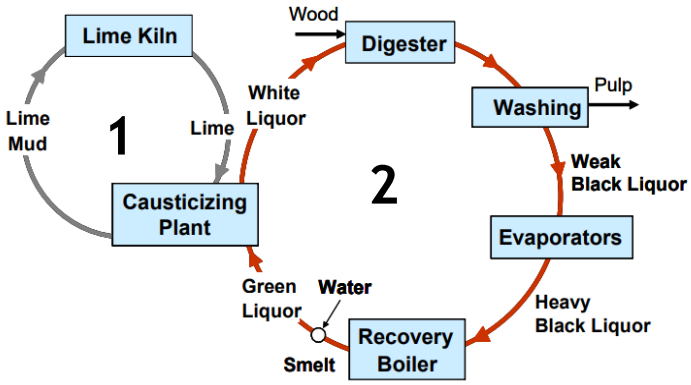

Figure 8 - Kraft recovery Process. Adapted from: The Kraft Chemical Recovery Process [27].

Figure 8 shows the kraft pulping process cycle. The main function of this process is the digestion of wood chips at elevated temperatures and pressure using a caustic water-based solvent. This process can be subdivided into two cycles, cycle (1) and cycle (2), strongly linked to each other. In cycle 2, the wood chips are fed to the digester and contacted with white liquor, a water solution of sodium sulfide (Na_2S) and sodium hydroxide (NaOH) with a pH between 13 – 14. At elevated temperatures (150 °C - 170 °C), the hydroxide and sulfide ions react with lignin and the carbohydrates, mainly glucomannans and xylans. In consequence, the cellulose fibres can be easily separated as solids from the dissolved lignin and hemicellulose [23, 27]. The pulp is washed using pulp mill condensates during the "brown-stock washing" process. The combined liquid fractions, a mixture of dissolved organic material and inorganic compounds, are called "weak" BL, illustrated in Figure 9. The washed pulp obtained will be transported to the bleaching plant if the bleached pulp is to be produced. The "weak" BL goes to the evaporation process, which will stepwise remove the water fraction, ending up in "strong" BL, with around 65 % of organic solids compounds, which will be incinerated in the recovery boiler to produce energy for the pulping process [23, 27]. The inorganic sodium and sulphur are recovered as molten smelt that consists mostly of (Na_2S) and sodium carbonate ($NaCO_3$), which are dissolved in water to form green liquor. The green liquor is then sent to the causticizing plant, where it reacts with lime and CaO to convert the $NaCO$ to NaOH. The causticized green liquor is known as "white liquor", which contains mostly NaOH and Na_2S, it is returned to the digester for reuse in pulping [23, 27]. The precipitated $CaCO$ (lime mud) from the causticizing reaction is washed and sent to a lime kiln, where it is heated to a high temperature to regenerate CaO.

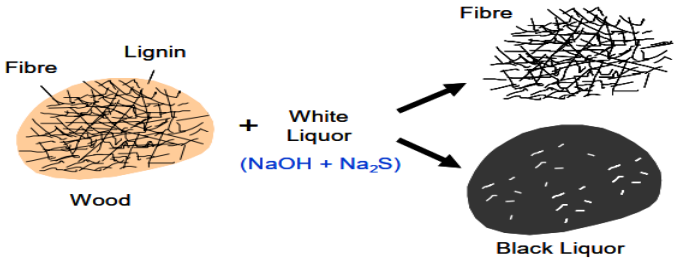

Figure 9 - Kraft pulping process products after the digestion step. Adapted from: The Kraft Chemical Recovery Process [27].

During years of optimisation, kraft pulp mills have turned from energy consumers to providers of green energy. The total energy demand has been reduced. In addition, the incineration of wood residues, including bark and energy wood, resulted in the capacity for lignin valorisation. Important to mention is that still around 80 % of lignin needs to be incinerated, while all cooking chemicals need to enter the recovery boiler [27].
Removal of lignin after the digester and prior to the recovery boiler is seen as an additional route to valuable products but also a way of reducing the load of the recovery boiler. This will enable the pulp to increase the pulp production rate [20].

2.5.2 Kraft Black Liquor

BL is a by-product from the separation of cellulose in paper pulp manufacturing, available in enormous quantities in the existing pulp mills. For every 1 ton of pulp production, approximately 7 tons of BL are produced in the kraft process; the BL is incinerated and produces 40-50 % more heat/electricity, used by the pulp mill itself, as was mentioned in the previous section [6, 27].
The BL composition is complex to characterise because BL is composed of hundreds of different organic compounds originating from all wood constituents (lignin, hemicellulose, tall oil). In addition, it has the inorganic cooking chemicals and their derivates [11].
Table 4 shows the principal differences between the pine kraft BL composition and the birch kraft BL, after the pulping process.
Noteworthy is the slightly low percentage of lignin in the birch wood black liquors, around 20 % less, compared to the kraft BL based in pine wood, on the other hand, it was detected more than 3.5 times residual polysaccharides, mainly xylan, in the birch wood black liquors [11].

Table 4 - *Kraft BL composition (% of dry matter) adapted from Energyforsk et al., Bajpai, Pratima et al., Lange, Heiko et al. [3, 11, 15].*

Component	Pine (wood)	Birch (wood)
Kraft Lignin	**31.0**	**25.0**
High molecular weight (>500 Da) fraction	28.0	22.0
Low molecular weight (<500 Da) fraction	3.0	3.0
Aliphatic carboxylic acids	**29.0**	**31.0**
Formic acid	6.0	4.0
Acetic acid	4.0	8.0
Other carboxylic acids (non-volatile, polar)	19.0	19.0
Other organics	**7.0**	**11.0**
Extractives	4.0	3.0
Polysaccharides	2.0	7.0
Miscellaneous	1.0	1.0
Inorganics	**33.0**	**33.0**
Sodium bound to organics	11.0	11.0
Inorganic compounds	22.0	22.0

The inorganic fraction in the BL needs to be considered. The inorganic salts present in BL are mainly dissolved in water. The salts dissolved in the BL derivate from the kraft cooking chemicals and their derivates, such as Na_2CO_3, $NaOH$, Na_2S and other sodium salts [11]. The percentage of different salts present in the pine kraft BL is shown in Table 5.
The salts derived from the kraft process typically need to be recycled back to the paper mill, but in some processes, they can have a key role; this hypothesis will be discussed in the next chapters.

Table 5 - Inorganic salts fraction in the pine kraft BL, adapted from: Energyforsk [11].

Inorganic Components	Percentage of inorganics (%)
NaOH	6.0
Na_2S	17.0
Na_2CO_3	32.0
Na_2SO_3	7.0
Na_2SO_4	12.0
$Na_2S_2O_3$	14.0
Others (K salts and chlorides)	12.0

2.5.3 Kraft lignin

Precipitation produced by acidification is widely used to remove kraft lignin from black liquor. The harsh alkaline environment to which lignin is subjected during this procedure causes substantial breakdown and repolymerisation processes. The resultant Kraft lignin includes thiol groups and is substantially condensed, with just a few ß-O-4 bonds left, which might make further valorisation difficult [1]. Figure 10 illustrates the model structure for softwood kraft lignin, in which the molecular formula has been reported, $C_9H_{8.5}O_{2.1}(OCH_3)_{0.8}(CO_2H)_{0.2}$ [12]. There are a lot of products that can be prepared from kraft lignin, for example, carbon fibres, phenolic resins, dispersants, binders, etc. In addition, some chemicals widely used in organic synthesis can be prepared from kraft lignin as well, especially benzene, vanillin, toluene, xylene, aldehydes, etc [19].

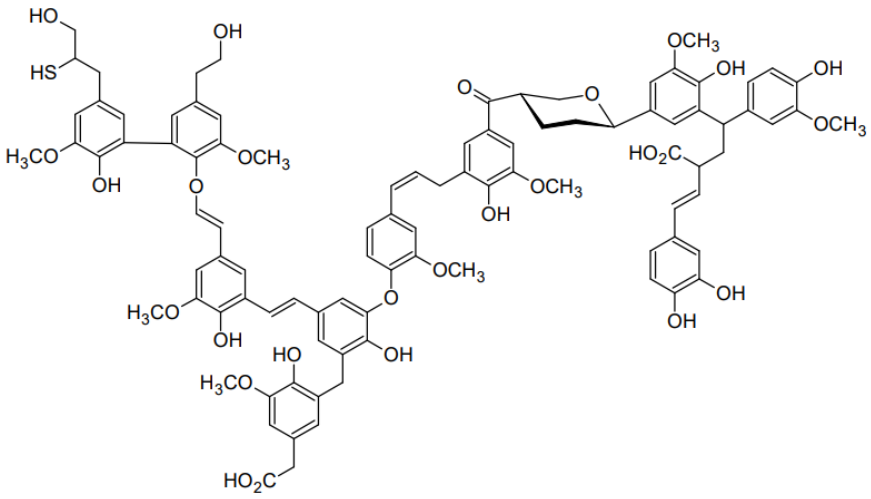

Figure 10 - Model Structure for softwood Kraft Lignin, adapted from Holady et al. [12].

2.6 Overview of Black Liquor Valorisation Techniques

2.6.1 Industrial Kraft Lignin Valorisation

Today, two valorisation routes for kraft lignin are industrially established. The first one is the incineration and energy production as part of the liquor cycle in every kraft mill [27]. As an alternative process, partial lignin precipitation and fractionation are commercialised as the so called Lignoboost process [4]. In this process, BL is acidified by adding CO_2 and inorganic acids, which results in the precipitation of kraft lignin. It is then washed, dried, and sold as a biobased polymer for low-value applications [4].

Applications to replace phenols in phenol-formaldehyde resins and asphalts have been quite successful. Additional applications of kraft lignin in its polymeric form include derivatisation to improve water solubility. Attempts to depolymerise lignin for monomers production are currently in the research stage. Those include solvolysis applying hydrogen donors, catalytic depolymerisation and electrochemical depolymerisation [10]. Most of those use lignin as starting material, which is in the first step redissolved in suitable solvents. Other routes, including pyrolysis and gasification, have either technical or economic challenges and experience less interest. Only a few of those publications propose the direct use of BL for lignin depolymerisation.

Oliveira et al. performed a Chronoamperometric and chronopotentiometric investigation of kraft black liquor, using Pt, Ni and AISI 304 SS electrodes to investigate the lignin oxidation process. In this publication, Ni was considering a promising electrode material for application in BL electrolysers [22, 24].

Jeremias et al. developed an electrochemical process for kraft BL valorisation, which used an electrolysis process [13]. This project studied the influence of several parameters, such as voltage applied in the electrolytic cell, temperature, and pH of the BL in the deposition of lignin at the anode. Nickel electrodes were used. The optimum operation conditions obtained were a cell voltage of 2.2 V, an electrolysis time of 4 h, a temperature of 55 °C and a pH between 5 and 8 for black liquor.

The high yield of the process, 80 % in terms of the mass of lignin deposited, when compared to the theoretical mass of lignin that could be deposited based on the volume of black liquor, and the maximum efficiency of 25.4 % [13, 21].

2.6.2 Outline of the Thesis

This thesis, as part of the H2020 EBIO project, aims to upgrade industrial bioliquids to produce platform chemicals and fuels. Specifically focussing on BL, the aim is to electrochemically oxidise and depolymerise lignin in the first step and consecutively is reduced electrochemically and catalytically. In the envisaged industrial process, this can be performed as a part of the condensation train. Fractions of BL will be injected in an electrochemical cycle. Valuable products are separated, and the remaining liquor is fed back to the evaporation train, as it is schematized in Figure 11.

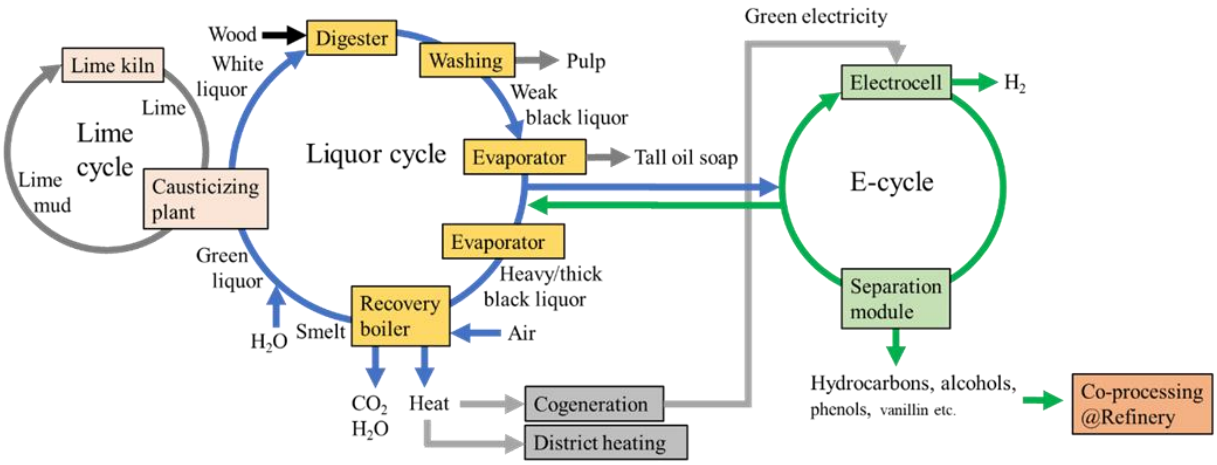

Figure 11 – Kraft process in combination with the proposed E-cycle by the H2020 EBIO project.

If operated at conditions comparable to those applied in the evaporation train, it can be implemented without significant changes in the kraft process. Produced hydrogen can be valorised as fuel. The electrochemical conversion will be developed as an alternative for lignin valorisation. Within this thesis, intermediate BL will be evaluated for electrochemical conversion. The thesis focuses on the evaluation of electrode materials and process parameters, including temperature, liquid flow rate, applied voltage and BL thickness. As a result, an operational window will be established as a basis for detailed optimisation and scale-up.

3 Materials and Methods

This chapter discusses all materials and methods applied within the framework of this thesis will be presented. The established setup is described along with the experimental methodology of calibration, electrochemical testing, and product analysis.

3.1 Industrial black liquor as feedstock

The BL used in the experiments was provided by Stora Enso's Sunila kraft pulp mill in Finland. This BL is an intermediate BL, which is industrially fed to the Lignoboost process for lignin precipitation and valorisation. It has already undergone some water removal by evaporation, having a solids content of 30 %. In addition, the tall oil soaps have been separated. This BL sample of 30 litres, shown in Figure 12 (left), is stored in a chemical storage room. No change in composition and molecular weight has been found during storage so far, and no sedimentation or phase separation has been observed either. Around three litres of BL were sampled to perform all experiments of the thesis, Figure 12 (right).

Figure 12 – Sample given Scandinavian Pulp Industry, blue barrel (left) and Laboratory bottle (right).

3.2 Electrode materials

As electrode materials, copper (Cu), nickel (Ni) and stainless steel (SS) have been applied in the form of metal sheets, which were cut for fitting into the cell. All three materials were tested as cathodes, but only nickel was used as anode. The nickel and copper sheets

were cut in the in-house workshop and flattened to ensure good packaging of the stack and avoid leaking of BL. Stainless steel cathode dimensions and design are represented in *Figure 15* and described in the following sections. The nickel and copper cathode dimensions and design are shown in Figure 13 and Figure 14. They were designed to enable simple packing and easy clamping of crocodile clamps of the power supply.

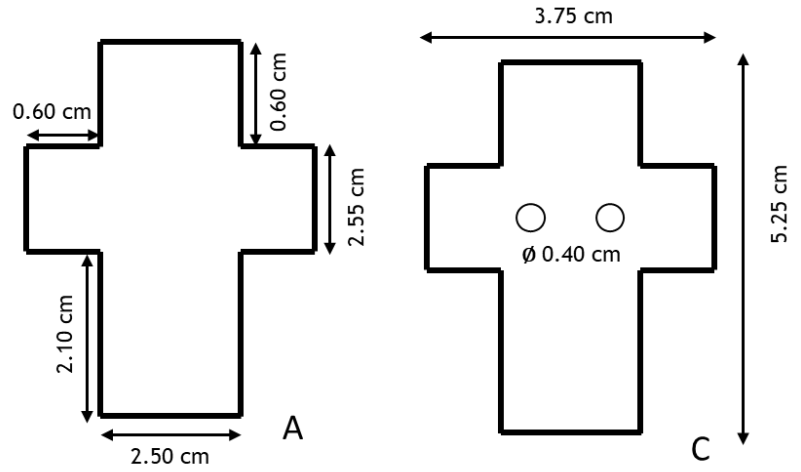

Figure 13 – Electrode design and dimensions, Anode (A) and Cathode (C).

Figure 14 shows the pictures of all the tested electrodes, designs and formats for both the anode and cathode tested.

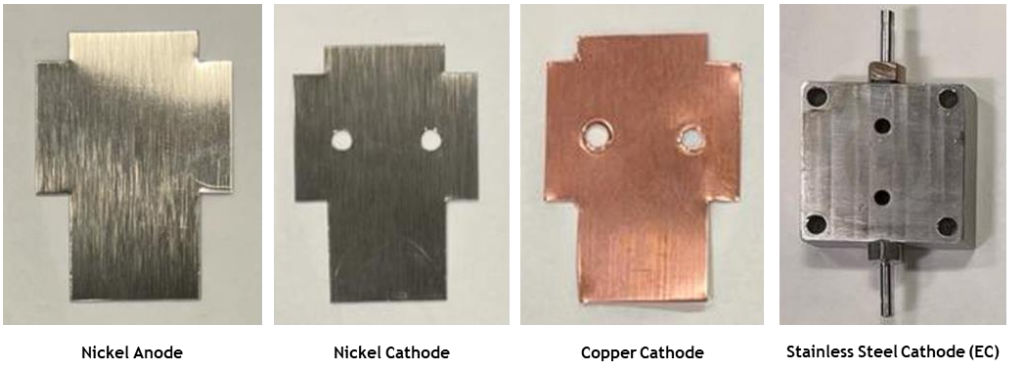

Figure 14 – Electrode materials used, Anode and Cathode, type of materials and electrode formats.

3.3 Electrochemical cell

The electrochemical cell (EC) used was prepared at SINTEF, inspired by the EC series *SSZ Electrolysers*, designed by the German company *Condias*. Teflon sheets were applied, both as spacers, but also to define the liquid volume between the electrodes, as shown in

Figure 15. The electrode area in contact with the liquid is 3.14 cm^2 each. The Teflon sheets assured the perfect isolation in all sections and good reusability during all the experiments; the thickness of each sheet is 0.150 cm, which was regularly validated.
The layers were held in place using insulated metal screws, as shown in *Figure 16*. Liquid inlet and outlet were placed at the bottom and top, respectively, to facilitate the removal of any gas bubbles by the liquid flow.

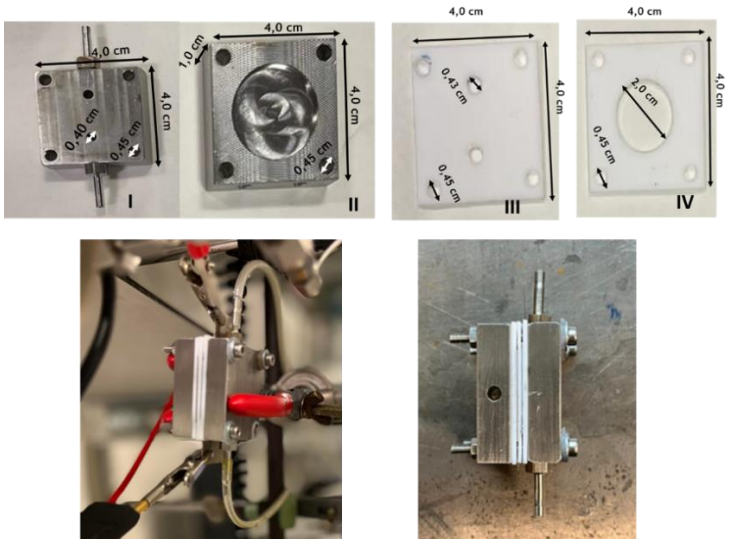

Figure 15 – EC Cathode section (I) and Anode section (II). Teflon Sheets (III) used between the cathode section (I) and the electrode (cathode), Teflon sheet (IV) used between each electrode and below the assembled EC.

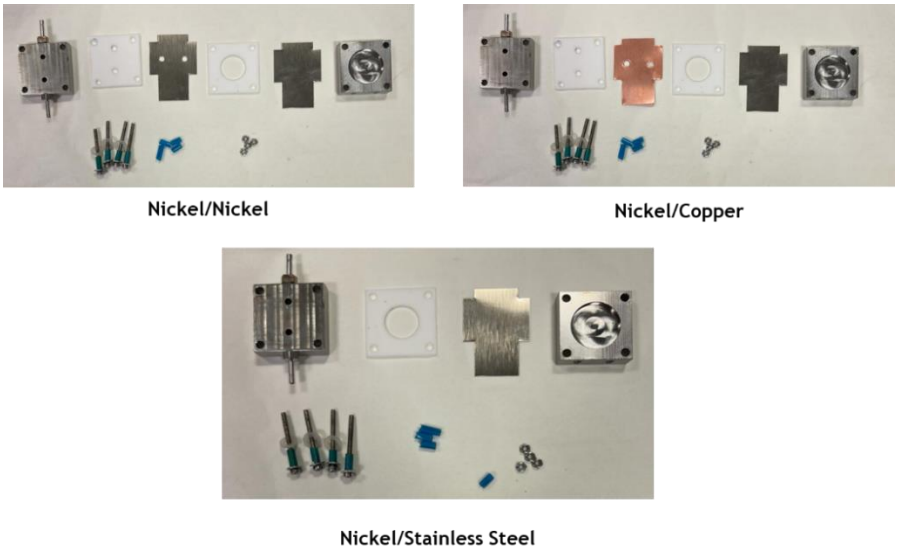

Figure 16 – EC configuration based in the electrode composition.

3.4 Experimental Setup

The experimental tests were conducted in a small-scale laboratory test rig, schematized in Figure 17.

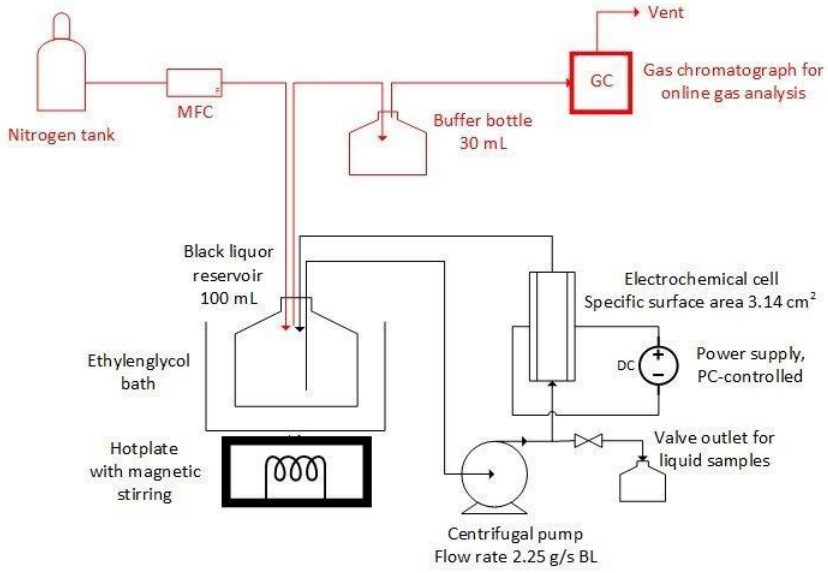

Figure 17 - Scheme of experimental setup for Lignin Electrochemical Depolymerisation.

The heart of the setup is the EC, in which the electrochemical conversion occurs. A Duran bottle with a 100 mL was used as a BL reservoir. Two different volumes of BL, 10 mL and 40 mL were circulated through the pump, cell and back to the bottle, as shown in Figure 14 by the black arrows. For the BL circulation, a centrifugal Pump was applied. A valve outlet for liquid samples was placed between the centrifugal pump and the EC. The liquid samples were later analysed using the techniques of High-Performance Liquid Chromatography (HPLC), Nuclear Magnetic Resonance (NMR) and Gel Permeation Chromatography (GPC). An ethylene glycol bath placed on a hot plate with a magnetic stirrer was used to heat the reservoir bottle of BL. Applying a bath temperature of 90 °C resulted in a BL temperature of 65 °C during circulation. Gas sampling was introduced by constantly flowing N_2 carrier gas through the reservoir bottle. As highlighted in red arrows, this gas stream is analysed online by GC. A buffer bottle was placed between the reservoir and the Gas Chromatography (GC) to prevent liquid products from entering the GC tubes. The voltage applied at the EC was supplied by a Power Supply Station, Aim-TTi QPX600DP Bench Power Supply, controlled by Test Bridge software.

3.5 Lab scale experiments

A comparable experimental procedure was established for the two types of experiments. The common steps performed are described below:

- Prepare the electrodes and EC assembly, and apply a flow of deionised water to validate that the cell is not leaking;
- In case no liquid leaks are detected, connect the inlet and outlet tubes to the pump and reservoir;
- Turn on the hot plate and magnetic strirrer and set the heating bath temperature to 90.0 ºC;
- Add defined amounts of BL and a magnetic stirrer to the reservoir bottle and place the bottle into the heating bath; based on the experiment typology there was the need to add a magnetic stringer to allow the mixing of BL during the experiments;
- Connect the carrier gas in and outflow to the reservoir bottle;
- After checking all the connections related to the gas phase, the centrifugal pump is started and the carrier gas flow is set to 5.3 % of the total flow range;
- Check the system pressure to be around 1.33 bar;
- Once the gas and liquid flows were stable, the GC analysis was initiated;
- The power supply was connected to the electrodes and the power supply program was started;
- The occurrence of foaming was observed during the initial 30 minutes of each experiment;

3.5.1 Calibration of black liquor circulation rate

The calibration curve for the circulation rate was obtained for the heated BL by using two reservoir bottles for out and inflow and placing the latter on a balance. The calibration curve is shown in Figure 18, demonstrating the influence of the voltage applied at the centrifugal pump. It was decided to conduct the electrochemical experiments at the highest available voltage resulting in a circulation rate of about 2 g/s. The calibration data are shown in Table 6, Table 7 and Table 8, Liquid Phase Equipment's appendix in section A.1.

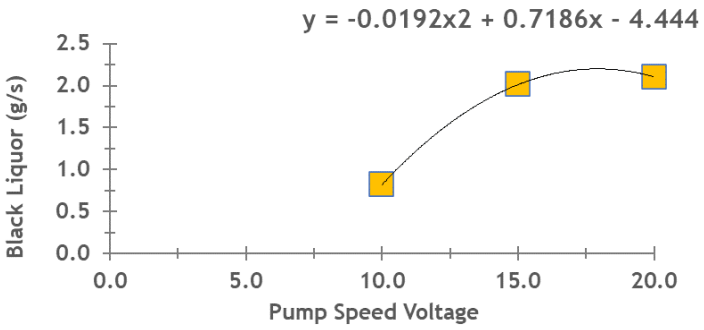

Figure 18 - Circulation rate calibration curve for the BL as function of the centrifugal pump voltage.

3.5.2 Chronoamperometry Step Tests

The chronoamperometry measurements were performed to study the effect of applied voltage on the cell current. This test can either be run by applying a slow voltage gradient or voltage steps, as shown on top of Figure 19. The Software Test Bridge was used to run the sequence. The voltage range applied was between 1.0 and 3.0 V, based on previous cyclic voltammetry studies performed at SINTEF. No reference electrode was applied. At every step, the voltage was kept constant for 20 minutes, after which the voltage was increased. During the test, the gas products were analysed by online GC with a sampling rate of 11 minutes.

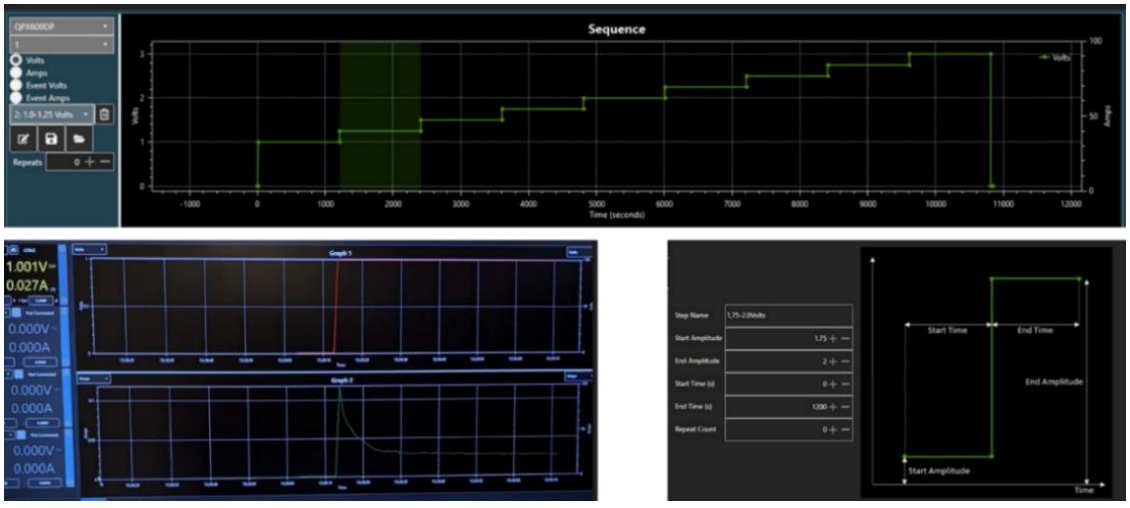

Figure 19 – Chronoamperometry step test sequence (on the Top) below it is represented the sequence modelling parameters (on the right side) and the programme Test bridge plots to analyse the voltage and current evolution during the experiments (left).

The experimental conditions of chronoamperometry step tests, according to the setup scheme in Figure 17 and Figure 20 are:

- **BL volume in black liquor reservoir:** 10.0 mL;
- **Duration of the Experiment:** 3:00 h;
- **BL Recirculation flow Rate:** 2.25 g/s;
- **Step Test Voltage Range:** 1.0; 1.25; 1.50; 1.75; 2.0; 2.25; 2.50; 3.00 V;
- **Time at each step:** 20.0 min;

3.5.3 Stability tests

After establishing a stable window of operation, stability tests were conducted. The objective of these tests was to evaluate the change of current, gas and liquid products over twelve hours. Due to this, a constant voltage was applied, as is in Figure 19. Gas products were analysed by online GC. Every two hours 1.0 mL of liquid sample was taken for offline liquid analysis by GPC, GC-MS and NMR, as described in the Product analysis section. The experimental conditions of stability tests according to the setup in Figure 17 and Figure 20 and based in Figure 19 are:

- **BL volume in black liquor reservoir:** 40.0 mL;
- **Duration of the Experiment:** 12 h;
- **BL Recirculation flow Rate:** 2.25 g/s;
- **BL Sampling at t** = 0; 2; 4; 6; 8; 10; 12 h;
- **Stability test Voltage:** Fixed voltage, based on the electrode couple, (Ni/Ni) (Ni/Cu) and /(Ni/SS);

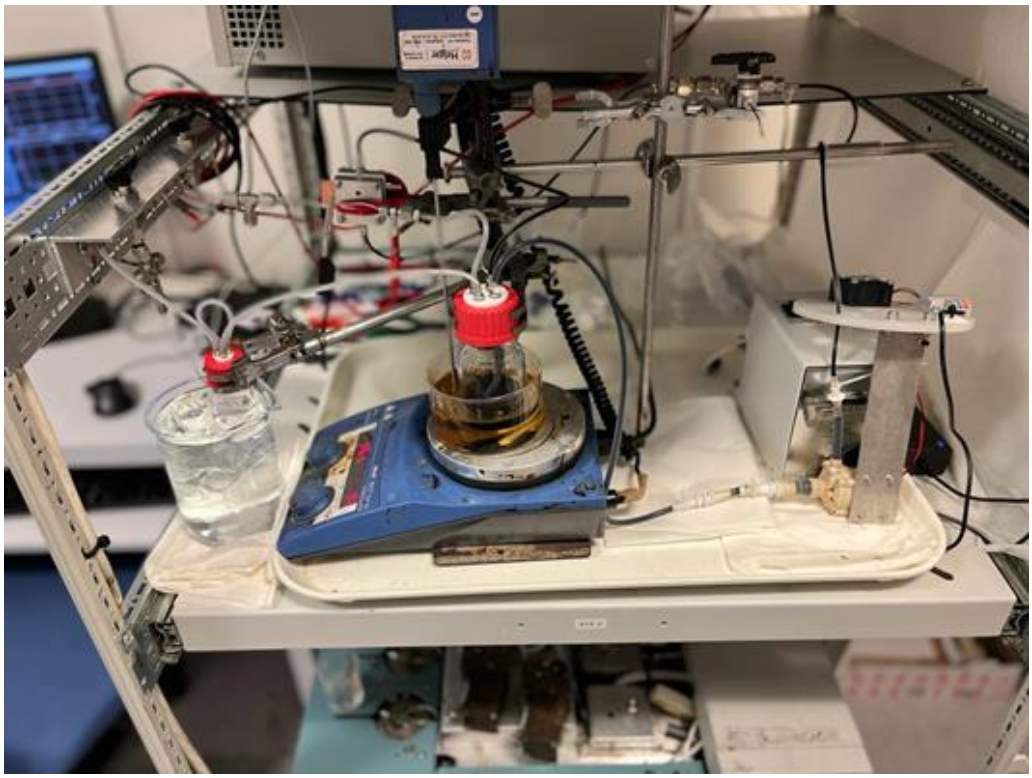

Figure 20 - Chronoamperometry Step test and Stability test experimental setup.

3.6 Product analysis

3.6.1 Online gas analysis by Gas Chromatography

During the electrochemical lignin conversion process, the gas products were analysed by GC. GC is an analytical method used to separate and quantify gas phase compounds based on their boiling point and/or chemical affinity to the chromatographic stationary phase. In our case, a gas carrier was flown at a constant flow rate through the BL reservoir bottle to dilute and carry gas products to the GC. The carrier gas used was nitrogen. Calibration of the flow rate was performed by applying a bubble flow meter. With the exact temperature and pressure, the gas flow rate at standard conditions was calculated for mass flow controller ranges of 2-10 % of total flow, as shown in Figure 21. Data from these measures are represented in Table 9 to 13, in appendix section A.2.

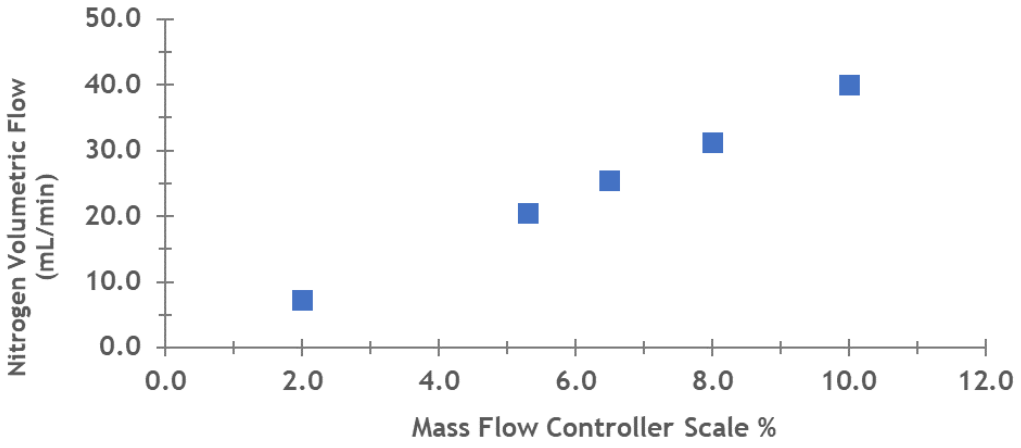

Figure 21 - Nitrogen carrier gas volumetric flow calibration as a function of the mass flow controller percentage.

For the electrochemical experiments, the mass flow controller setting of 5.3 % N_2 was applied, corresponding to a volumetric flow rate of 20.46 mL/min STP, as shown in Equations I and II.

$$\dot{V}_{N_2} = \frac{Volume}{time} = \frac{7.00}{20.71} = 0.34\, mL/s = 0.34 \times 60 = 20.28\ \mathrm{mL/min} \qquad \text{(Equation I)}$$

$$\dot{V}_{N_2\,(STP)} = \frac{P_1 \times \dot{V}_{N_2} \times T_2}{P_2 \times T_1} = \frac{102430 \times 20.51 \times 293.15}{101325 \times 297.15} = 20.46\ \mathrm{mL/min} \qquad \text{(Equation II)}$$

To perform the GC analysis, it was necessary to calibrate the GC for gas components of interest. The applied reference gas bottles contained nitrogen (N_2), hydrogen (H_2), oxygen (O_2), carbon dioxide(CO_2), carbon monoxide (CO), methane (CH_4) and methanol (CH_3OH); the concentration percentage (V/V) described in each reference gas bottle and the respective peak areas measured by the GC are listed in Table 14 to 17 in the appendix section A.2. Using those gas concentrations and the obtained peak areas, the concentration ratios (C/C) and peak area ratios (A/A) were calculated. They are listed in Table 18 in the appendix section A.2. Figure 22 shows the calibration curves for H_2 and O_2. Equations III and IV show the linear relationship between area ratios and concentration ratios.

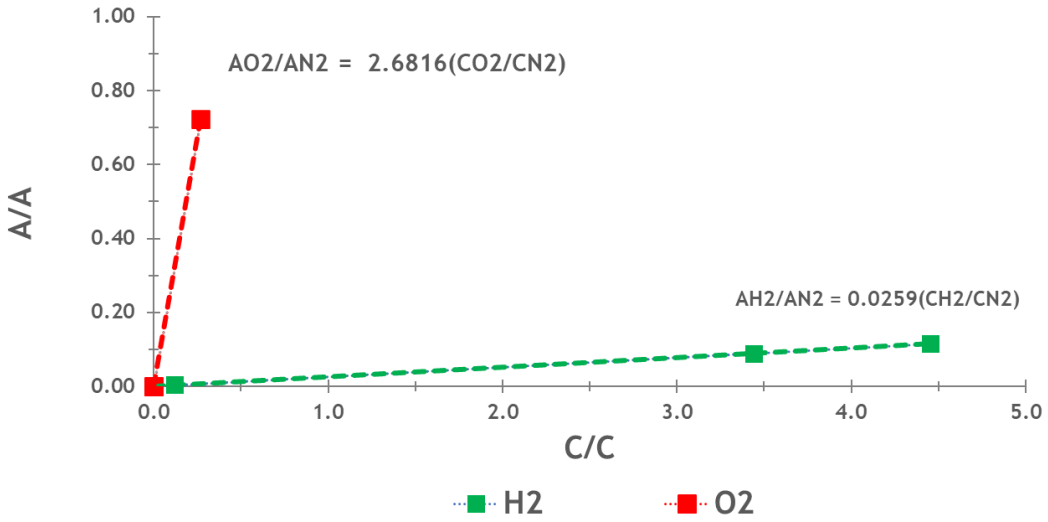

Figure 22 - Hydrogen (H2) and Oxygen (O2) GC gas peak areas ratio as a function of gas concentration ratio.

$$\frac{A(H_2)}{A(N_2)} = 0.0259\,\frac{C(H_2)}{C(N_2)} \Leftrightarrow \frac{C(H_2)}{C(N_2)} = \frac{\frac{A(H_2)}{A(N_2)}}{0.0259} \qquad \textit{(Equation III)}$$

$$\frac{A(O_2)}{A(N_2)} = 2.6816\,\frac{C(O_2)}{C(N_2)} \Leftrightarrow \frac{C(O_2)}{C(N_2)} = \frac{\frac{A(O_2)}{A(N_2)}}{2.6816} \qquad \text{(Equation IV)}$$

Using the concentration ratio for each gas and knowing the volumetric flow rate for the carrier gas at STP conditions, the volumetric flow rate of hydrogen and oxygen $(\mathrm{L/min})$ was calculated by Equation V.

$$\dot{V}(\mathrm{H_2}) = \frac{\mathrm{C(H_2)}}{\mathrm{C(N_2)}} \times 20.46 \times 10^{-3} \quad \text{and} \quad \dot{V}\,(\mathrm{O_2}) = \frac{\mathrm{C(O_2)}}{\mathrm{C(N_2)}} \times 20.46 \times 10^{-3} \qquad \text{(Equation V)}$$

In Equation VI, using the Ideal Gas Law Equation, considering R = 8.314 $\mathrm{m^3.Pa.K^{-1}.mol^{-1}}$, the carrier gas molar flow $(\dot{n})$ was calculated:

$$PV = NRT \Leftrightarrow \frac{V}{N} = \frac{RT}{P} \Leftrightarrow \frac{V}{N} = \frac{8.314 \times 293.15}{101325} = 24.05\ \mathrm{L/mol} \qquad \text{(Equation VI)}$$

Based on the carrier gas molar flow $(\dot{n})$, the molar flow for hydrogen and oxygen $(\mathrm{mol/s})$ can be obtained, as it is represented in Equation VII:

$$\dot{n}\,(\mathrm{H_2}) = \frac{\dot{V}(\mathrm{N_2})}{\frac{V}{N} \times 60} \quad \text{and} \quad \dot{n}\,(\mathrm{O_2}) = \frac{\dot{V}(\mathrm{O_2})}{\frac{V}{N} \times 60} \qquad \text{(Equation VII)}$$

Assuming water electrolysis the selectivity for hydrogen $S(\mathrm{H_2})$ and oxygen $S(\mathrm{O_2})$ are calculated from the measured current, the Faradaic constant 96485.3321 A.s/mol and molar flow (mol/min), as it is represented in Equations VIII to Equation XI:

$$\mathrm{AH_2\,(A)} = 2 \times \dot{\mathrm{n}}\,(\mathrm{H_2}) \times 96485.3321 \qquad \text{(Equation VIII)}$$

$$AO_2\,(A) = 4 \times \dot{n}\,(O_2) \times 96485.3321 \qquad \text{(Equation IX)}$$

$$\text{Selectivity } (SH_2) = \frac{AH_2}{\text{Measured } Current} \times 100 \qquad \text{(Equation X)}$$

$$\text{Selectivity } (SO_2) = \frac{AO_2}{\text{Measured } Current} \times 100 \qquad \text{(Equation XI)}$$

3.6.2 Molecular weight distribution measurements

Size exclusion chromatography (SEC) was applied to analyse the molecular weight distribution of the samples. An Agilent HPLC 1100 instrument was equipped with a guard column and two PL aquagel-OH MIXED-H 8 μm 30x7.5 mm SEC columns. As an eluent, an aqueous solution of 0.27g/L NaN and 0.2g/L NaOH was applied. At a flow rate of 0.9 mL/min and a temperature of 30 °C the samples were analysed by DAD in the wavelength range of 190-400 and by RID. The samples were dissolved in the eluent in a ratio mass ratio of 1:15, ensuring complete dissolution. Commercial sulfonated polystyrene standards were used as standards for molecular weight distribution.

3.6.3 CNMR analysis of samples

The experimental procedure required to obtain the NMR spectra was straightforward. The samples were dissolved in or mixed with a suitable deuterated solvent (in this case – D_2O: ca 300 mg was dissolved in ca 1.0 g of D_2O). A small amount of reference compound was added, and for D_2O samples TMS-salt (DSS) was used. The standard size of the sample tube for routine 1H and 13C experiments is 5 mm OD (outside diameter), and this requires 0.7 mL of solution. The amount of sample required for all NMR measurements is high compared with other spectroscopic techniques, such as infrared and ultraviolet spectroscopy. Especially for 13C measurements, sensitivity problems are such that much more sample is required than for proton NMR.

3.6.4 Monomers identification by gas chromatography

BL samples from stability tests were diluted in water, then neutralised by adding diluted HCL and subsequently extracted using ethyl acetate. After vacuum distillation of ethyl acetate, the remaining residues were redissolved in tetrahydrofuran, spiked with 1 % (w/w) decane as an external standard. The prepared samples were analysed using a gas chromatograph connected with a mass spectrometer and a flame ionization detector (FID) on an Agilent GC×GC-MS/FID system. The MS detector was applied to identify the compounds, and the identified compounds were quantified by FID, using the FID response

factors described by de Saint Laumer et al. [5]. The FID signals of the identified compounds accounted for more than 98 % of the total sum of signals detected.

4 Results and Discussion

In this chapter, the experimental results are discussed. This chapter is divided into three sections: Initial tests of operational parameters, chronoamperometry step tests and stability tests, describing an initial screening of the operational regime and studies of the medium term electrode stability.

4.1 Effect of experimental conditions

As an initial test, the effect of the circulation pump speed on the mass transfer rate at the electrode surface and eventually the current was evaluated. Figure 23 (left) shows the current applying a Nickel/Stainless Steel electrode combination during 90 min of electrochemical conversion, at 2.0 Volts. An initial circulation rate of 2.1 g/s of BL (Region A) was applied. After 30 min the circulation rate was decreased to 2.0 g/s of BL (Region B). After another 60 min. the pump speed voltage was again decreased to 0.8 g/s of BL (Region C). Figure 23 shows that the resulting current for regions A-C decreases as the circulation rate decreases. This clearly shows an operation in the liquid-solid mass transfer limited regime, certainly of either lignin transport to or product transport from the electrode surface. The currents are rather constant for each region, suggesting no formation of a deposition layer. This is confirmed by visual observation of the electrode surfaces in Figure 23 (right).

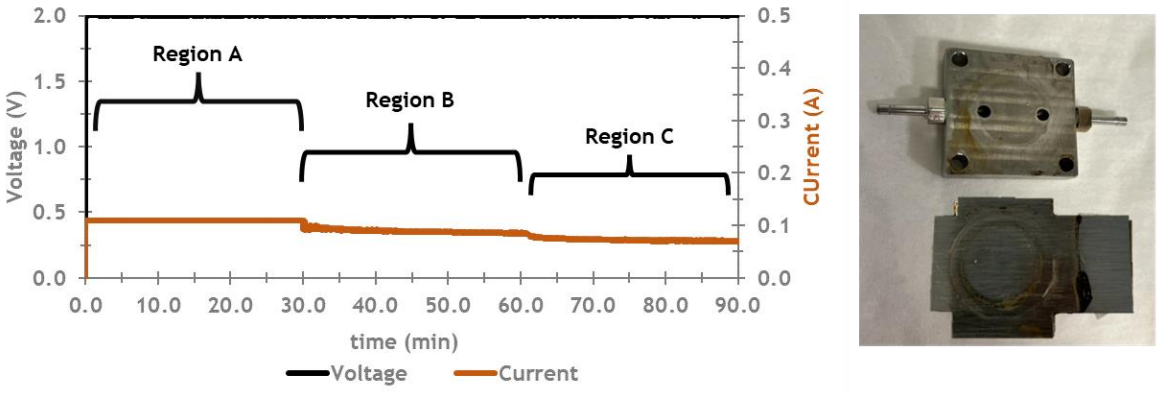

Figure 23 - Effect of the BL circulation rate on the current generated during the electrochemical reaction tested at 2.0 Volts for the electrode combination Ni/SS, left side.

Based on this, in the following experiments, a circulation rate of 2.0 g/s of BL was applied.

4.2 Chronoamperometry step test

The chronoamperometry tests of the three electrode combinations, Ni/SS, Ni/Ni and Ni/Cu, are presented in Figure 24. For every electrode combination, three distinct regions can be identified. In the first region, marked in light blue, the current is close to zero. During this initial stage, strong current fluctuations are observed. During this period, strong foaming of the BL in the reservoir bottle is observed. This foaming is observed at each experiment when applying fresh electrodes and BL, both at low and higher voltages applied. This will be further discussed in section 4.4.

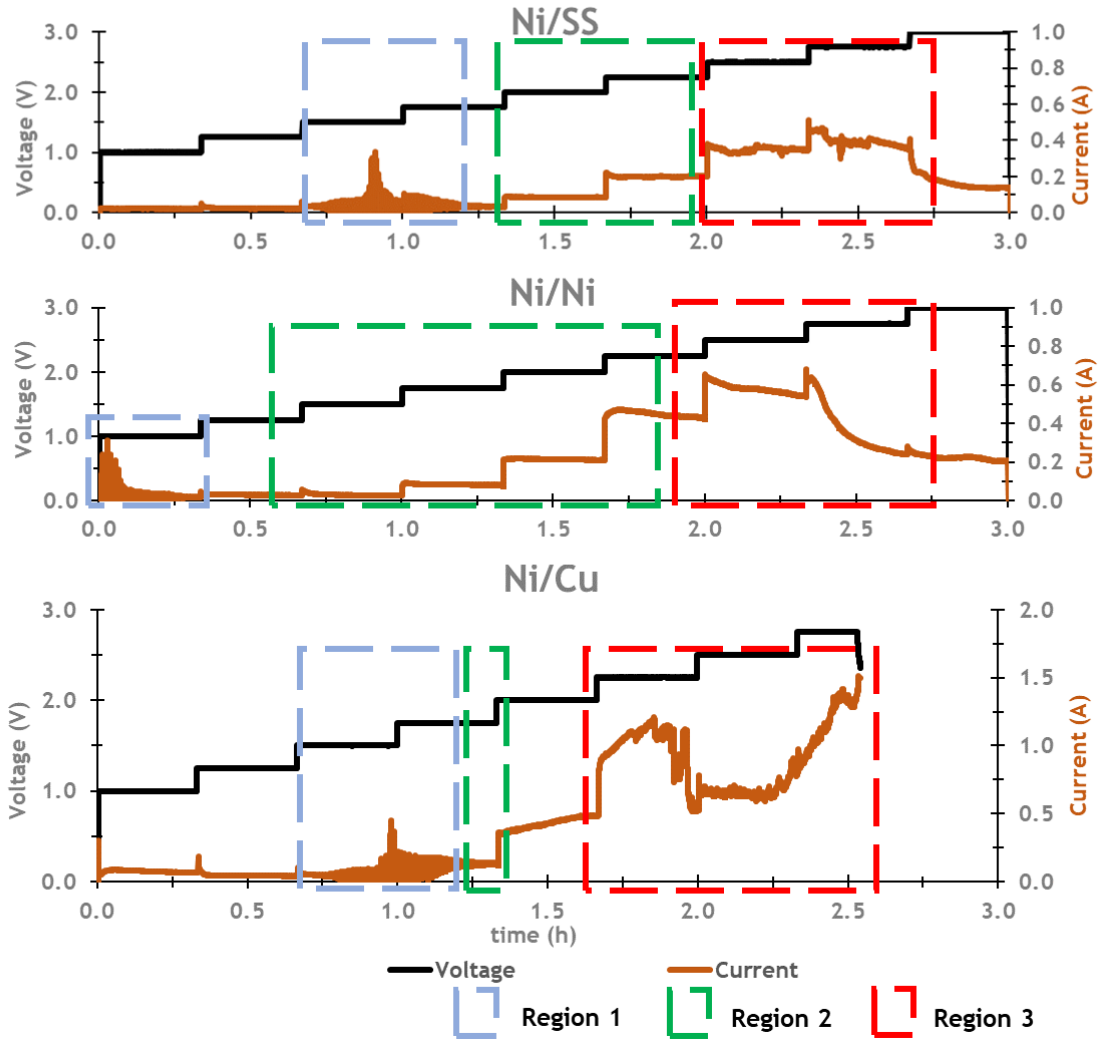

Figure 24 - Chronoamperometry step test representing the current (A) evolution as a function of the applied potential (V), tested for the three studied electrode combinations: Ni/Ni, Ni/SS and Ni/Cu.

The second region, highlighted in green, is characterised by a rather constant current and voltages, which are high enough for industrial electrochemical conversion. Ni/Ni shows the largest extent of this region with the highest currents of up to 0.5 A. Even higher currents result in unstable currents, as shown in the third region, marked in red. For the case of Ni/Ni, a rapid current drop is observed. For the case of Ni/Cu and Ni/SS, strong current jumps are observed. Figure 25 shows the electrode surfaces after the test. In all cases, deposit formation is observed, which is especially strong for the cases of Ni/Ni and Ni/Cu. Most deposits are formed on the cathodes, where the concentration of OH^- should be higher. This means that it is not just lignin that is precipitated due to pH reduction. Instead, those deposits are precipitated from BL, either due to a significantly different chemical composition or due to a significantly higher molecular mass.

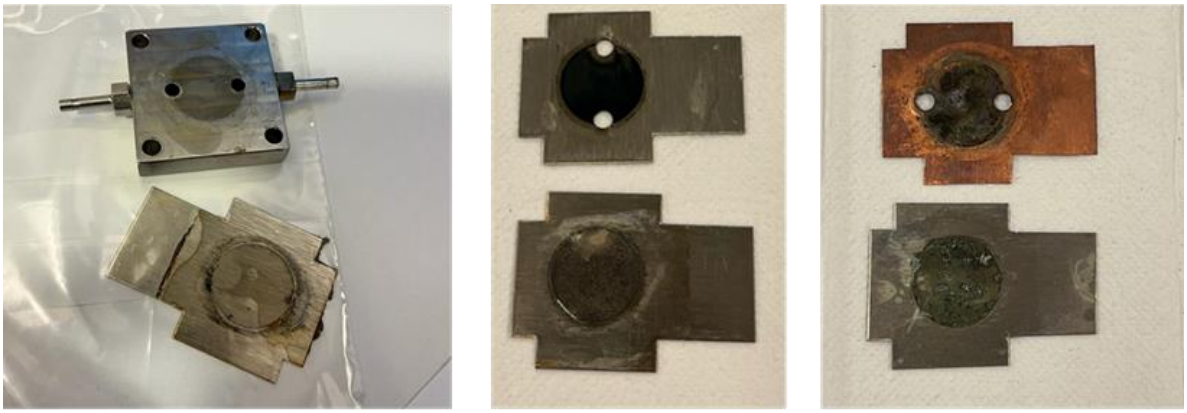

Figure 25 – Electrode surface pictures after the chronoamperometry step test.

In consequence, BL conversion using those electrode materials should avoid operating in region three. The operation should be performed in constant voltage mode. When running the cell in constant current, entering this region would cause rapid electrode deposit formation, which would further be accelerated when trying to increase the voltage to keep the current constant.

The chronoamperometry step test results enable us to plot the current as a function of the applied potential, for each combination of electrodes, shown in Figure 26. Region A, highlighted by the black square at the left, shows currents close to zero when applying voltages below 2.0 V. The voltage required for a relevant electrochemical conversion should be found between 1.5 and 2.0 V for all three electrode combinations. Applying

nickel as anode material in all three cases indicates that the anodic process is certainly rate limiting. Region B, the red square on the right of Figure 26, can be characterized by a deviation from a linear curve and highly unstable performance. Those processes must not be operated at voltages higher than 2.5 V, as was already verified in region 3 of Figure 24.

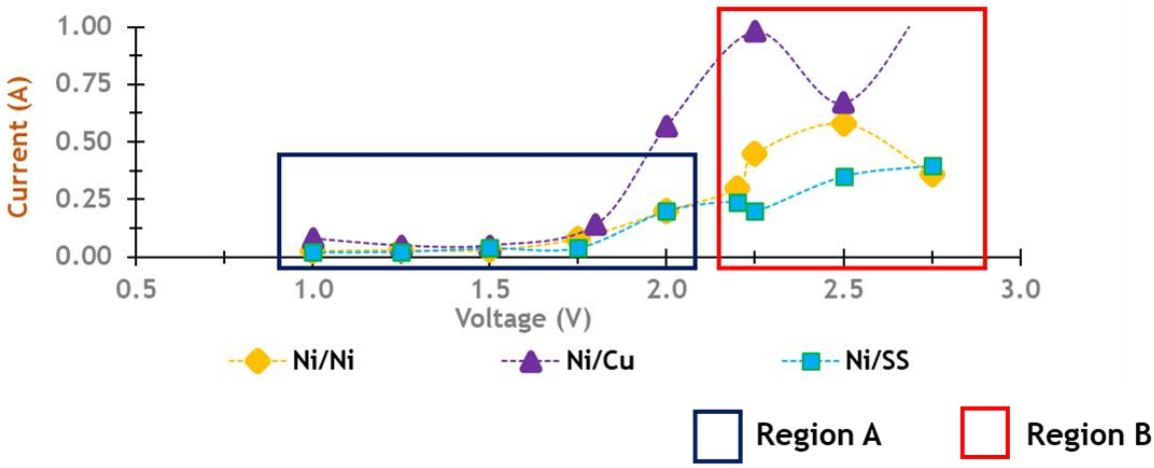

Figure 26 - Current as a function of the applied voltage for the three electrode combinations, right side. On the left side, it is represented the current obtained values for a small potential range.

4.3 Constant voltage stability test

Based on the identified regions of stable currents obtained by the chronoamperometry step tests, stability tests were performed to evaluate the performance over several hours and analyse the reaction products in gas and liquid phases.

4.3.1 Nickel/Stainless Steal

The experimental data for Ni/SS are shown in Figure 27 and Figure 28, both obtained currently for the given voltages of 2.0 and 2.2 V. Those values were chosen based on the stability tests of section 4.2, representing values within the stable region B Figure 24 and 26. In both Figure 27 and Figure 28, a comparable behaviour can be observed. After an initialisation phase, including an unstable region of foaming, the current slowly drops. The hydrogen evolution shows a similar trend. The oxygen evolution is nearly fully suppressed for 2.2 V, while for 2.0 V a slow increase of the faradaic efficiency towards oxygen production is observed. NMR data do not show a significant increase in carboxylic carbon, meaning that the full oxidation to CO_2 is not significant either. This means that the oxidation is rather selective towards lignin.

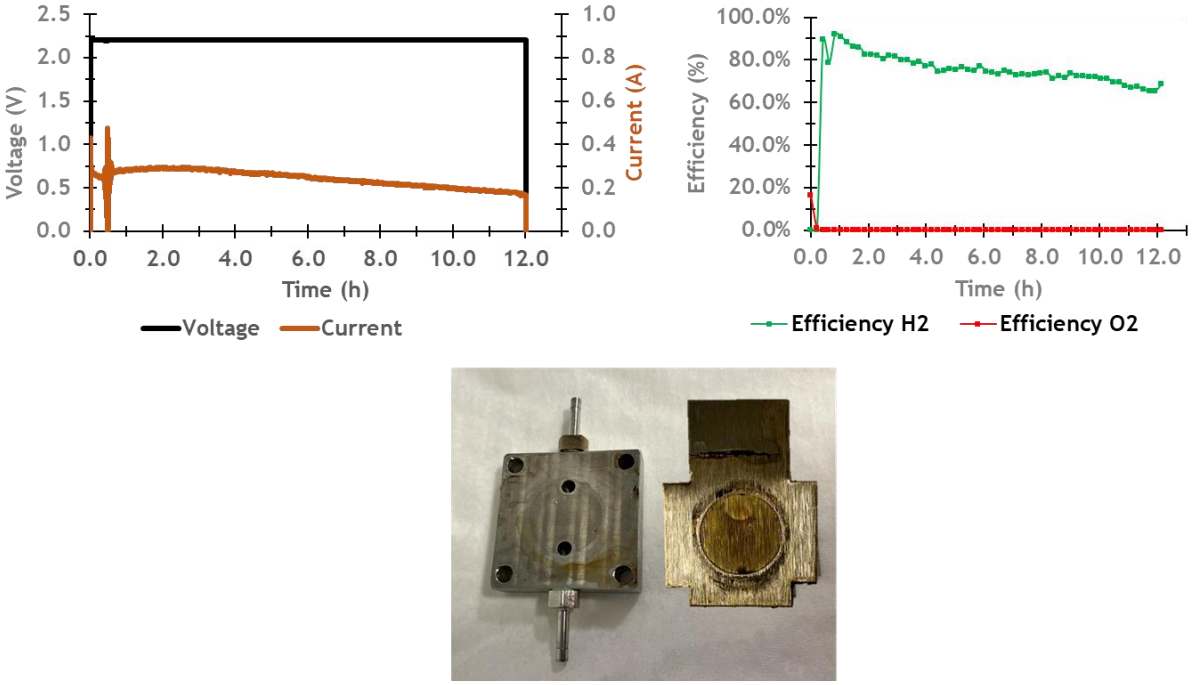

Figure 27 – Nickel/Stainless Steel stability test at 2.20 Volts, where it is represented the relationship between the applied voltage and the originated current during the 12 hours of experiment, on the top on, the left side. On the right side, the hydrogen and oxygen efficiency evolution during the 12 hours and at the bottom the electrode surface aspect after 12 hours of stability test.

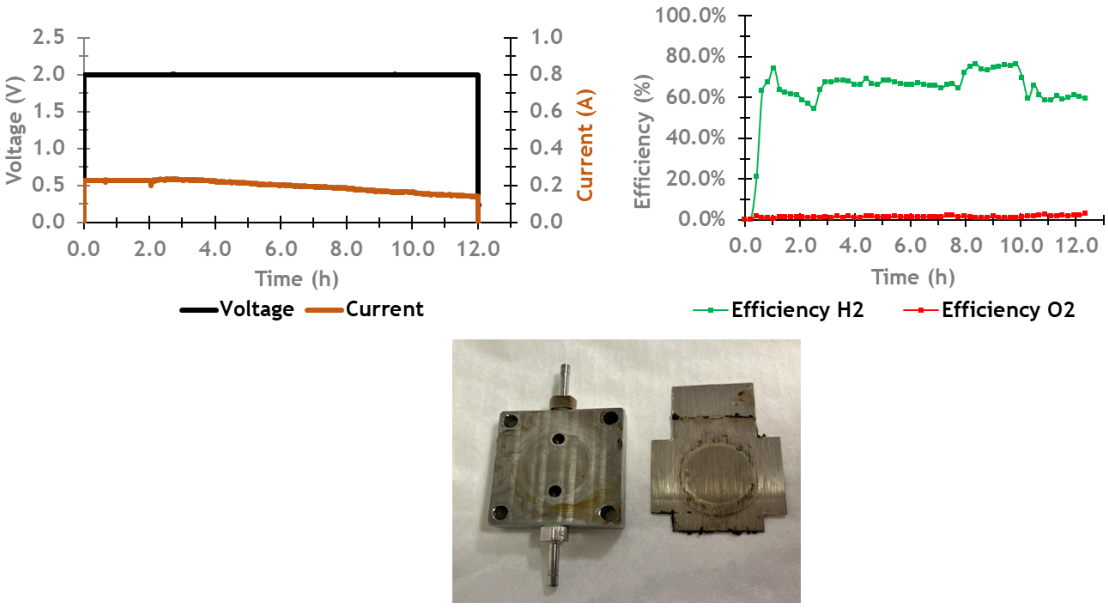

Figure 28 – Nickel/Stainless Steel stability test at 2.0 Volts, where it is represented the relationship between the applied voltage and the originated current during the 12 hours of experiment, on the top, left side. On the right side, the hydrogen and oxygen efficiency evolution during the 12 hours and at the bottom the electrode surface aspect after 12 hours of stability test.

4.3.2 Nickel/Nickel

In the case of nickel as both anode and cathode, Figure 29 and Figure 30, again an unstable region of foam formation is observed at around 30 min. After this, the current drops steeply while the hydrogen production increases to values above 100 % if water electrolysis is assumed. This means that significant amounts of carbon are formed at the cathode surface. Interestingly for the test applying 2.0 V, the hydrogen evolution is delayed for some minutes, before the hydrogen production significantly rises. Nickel cathodes are known to be highly selective to hydrogen evolution. Further investigation into the mechanisms and products/intermediates formed during this initial phase needs to be studied in more detail. Oxygen evolution is low, like in the Ni/SS case. This is expected as the same electrode material was applied. Deposits formation at the electrodes is rather severe when a voltage of 2.2 V is applied, while for 2.0 V only spots of carbon deposits are found at the electrodes.

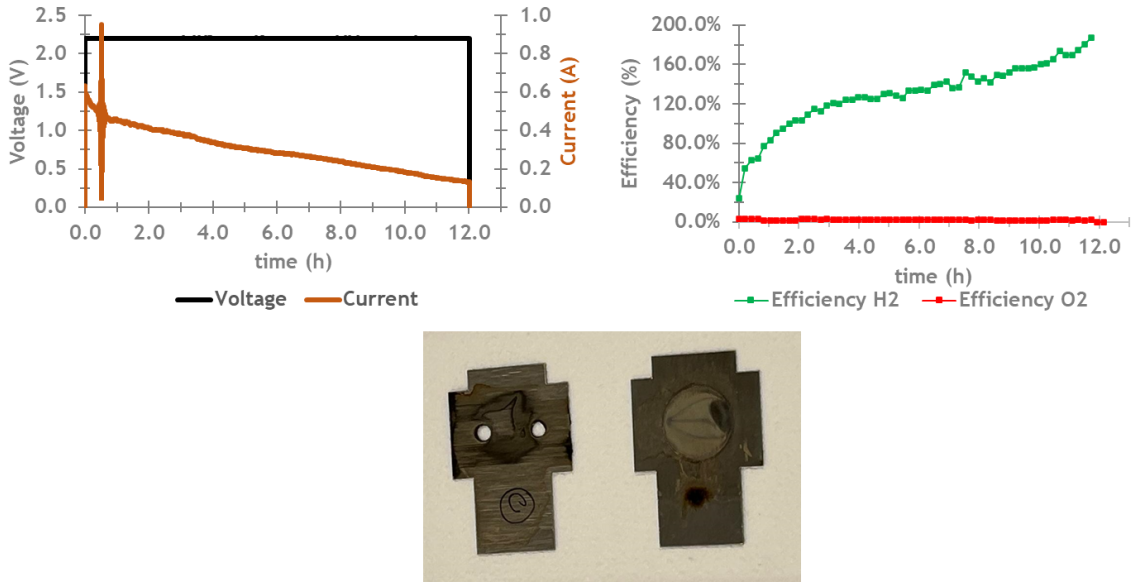

Figure 29 – Nickel/Nickel Stability test at 2.20 Volts, where it is represented the relationship between the applied voltage and the originated current during the 12 hours of experiment, on the top, left side. On the right side, the hydrogen and oxygen efficiency evolution during the 12 hours and at the bottom the electrode surface aspect after 12 hours of stability test.

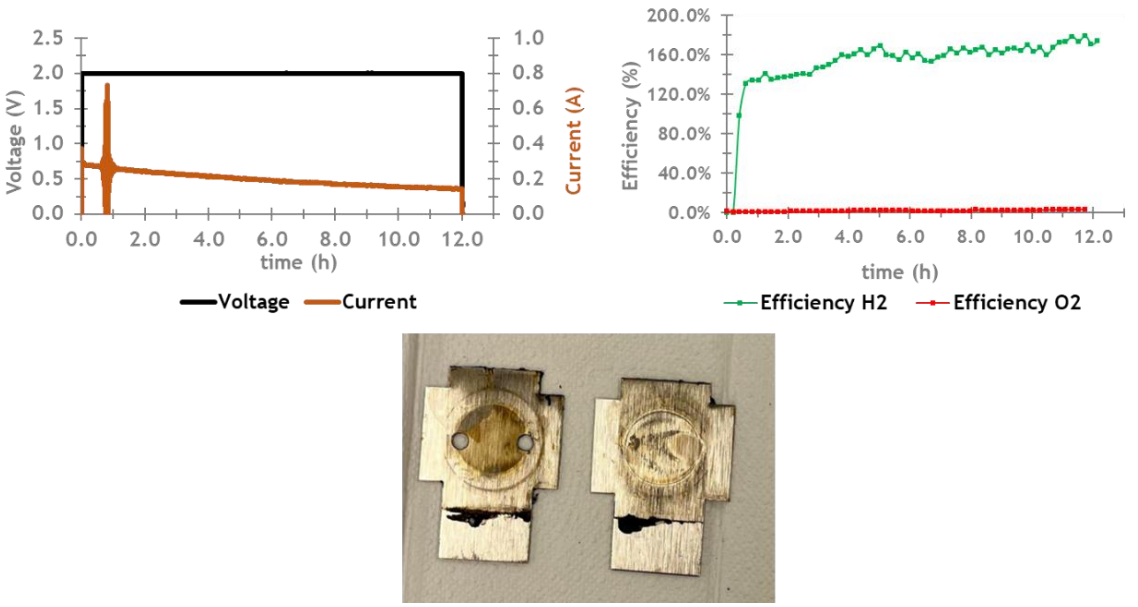

Figure 30 – Nickel/Nickel Stability test at 2.0 Volts, where it is represented the relationship between the applied voltage and the originated current during the 12 hours of experiment, on the top, left side. On the right side, the hydrogen and oxygen efficiency evolution during the 12 hours and at the bottom the electrode surface aspect after 12 hours of stability test.

4.3.3 Nickel/Copper

For the 2.0 V tests combining Ni/Cu, Figure 31, a highly unstable current is observed during the entire run, despite the rather stable performance during the chronoamperometric tests. This poses challenges for a possible industrial operation. Similar to the Ni/Ni case, a delay in hydrogen evolution is observed. Copper is known for a low selectivity of hydrogen evolution, which is in line with the initial observation. Once certain deposits are formed then this behaviour seems suppressed, and carbonisation takes over, resulting in a high formation rate of hydrogen and deposits. The nature of those deposits is currently under investigation by applying both NMR and SEM-EDS.

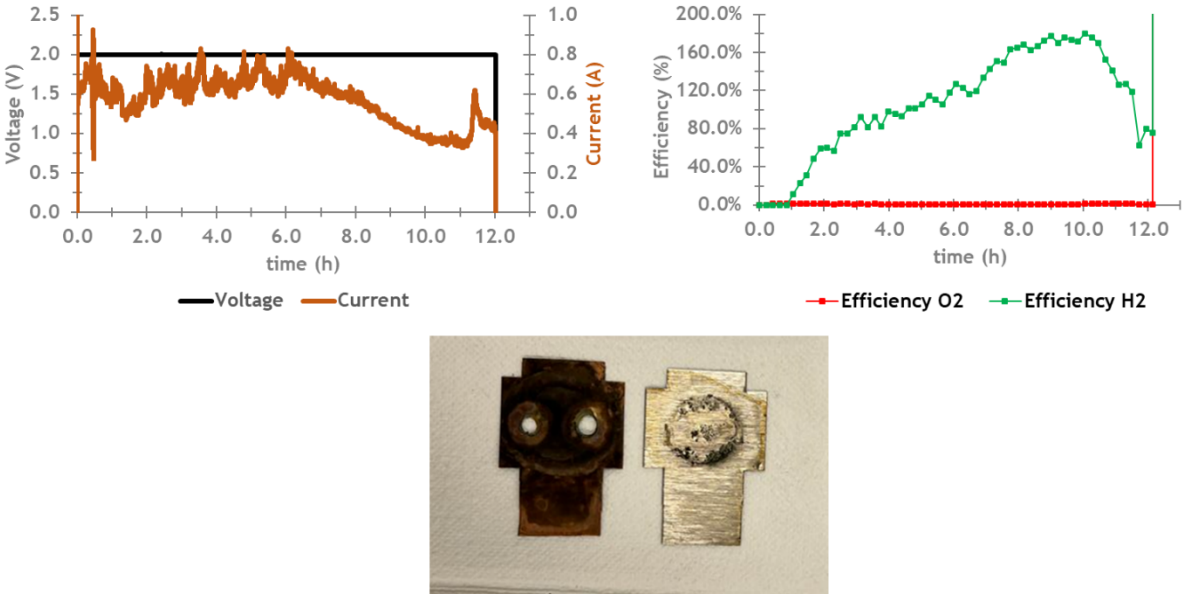

Figure 31 - Nickel/Copper Stability test at 2.0 Volts, where it is represented the relationship between the applied voltage and the originated current during the 12 hours of experiment, on the top, left side. On the right side, the hydrogen and oxygen efficiency evolution during the 12 hours and at the bottom the electrode surface aspect after 12 hours of stability test.

4.4 Product analysis

GPC data give a good insight into the reaction mechanisms by tracking the changes in the molecular weight distribution during the stability experiments. Figure 32 shows the GPC-RID chromatogram for the feedstock black liquor and the product samples taken every 2 hours. It shows the entire range of polymeric, oligomeric, and monomeric compounds of lignin and cellulosic origin in the retention times window between 17 and 21 minutes. The peaks with retention times from 22 minutes onwards can be assigned to smaller acids, including acetic and formic acids. Electrochemical conversion products show a significant change in the chromatogram. Especially the phenolic monomers are absent while the intensities of polymeric fractions are increased. It is observed that the polymeric fraction having the peak at 19 minutes is increasing with the conversion time, especially for the experiments applying nickel and copper cathodes. This means that lignin condensation reactions producing large polymeric compounds are the dominant reactions.

C^{13}-NMR, Figure 36 Figure 39, found in appendix B.1, have not revealed significant changes in the liquid phase carbon. This means that neither significant oxidation of the dissolved lignin has occurred, nor has significant amounts of additional CO_2 been dissolved. This

supports the hypothesis that lignin condensation is the dominant conversion process. Still, the characterisation of the electrode deposits is in progress.

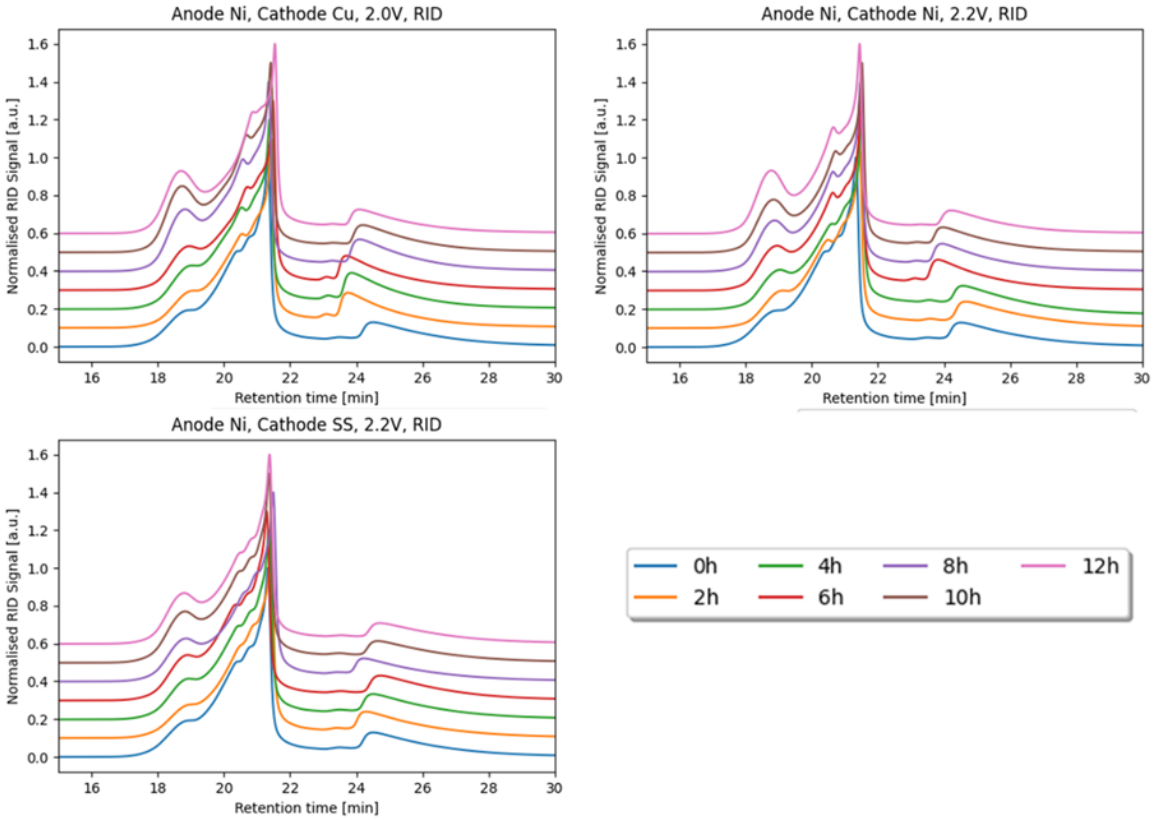

Figure 32 – GPC-RID chromatograms of 12 hours test samples for three electrode combinations.

GC-MS/FID gives a complimentary analysis of the origin and conversion of monomeric compounds. In Figure 33, the chromatograms are presented for BL feedstock as well as the products after 12 hours of operation.

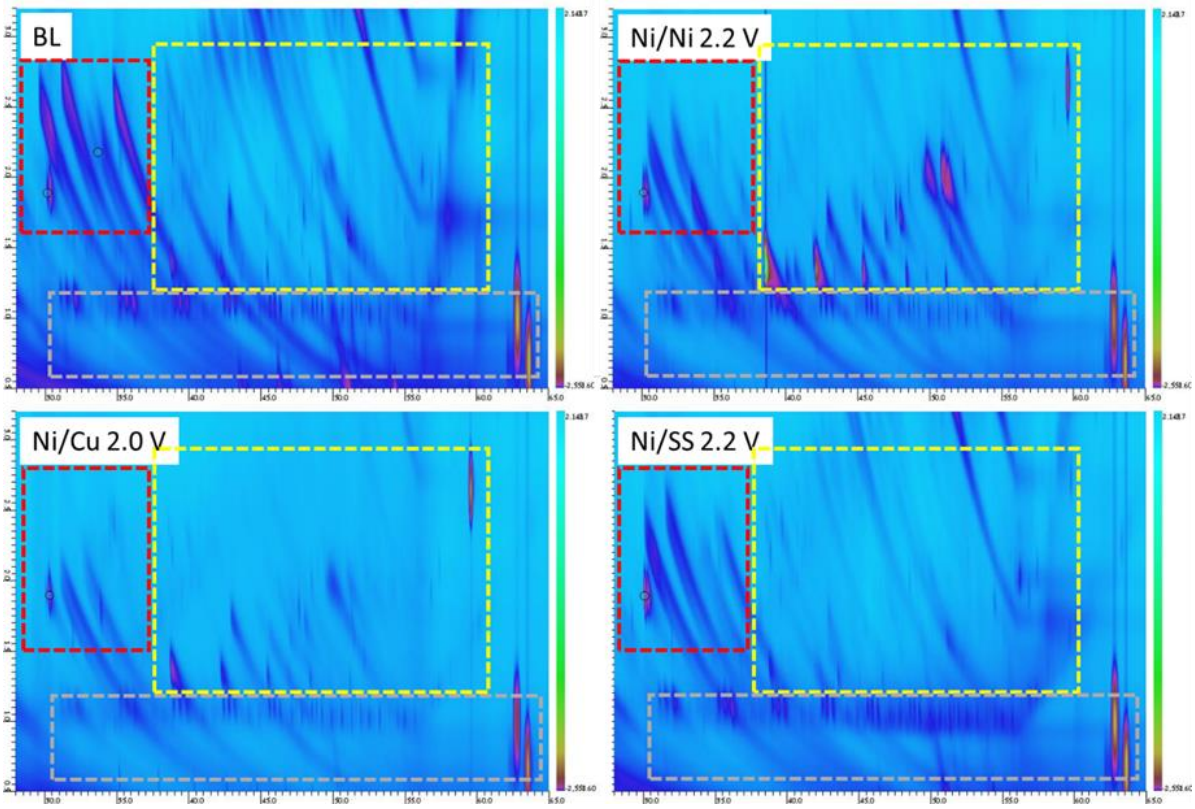

Figure 33 – GC-FID chromatographs for BL feedstock and 12 hours conversion tests. The highlighted areas are left/red – phenolic monomers of lignitic origin; right/yellow – alkyl methyl esters; bottom/grey – solvent impurities.

It is observed that the monomeric lignin-based phenolics (vanillin, acetovanillin, guaiacol etc.) are present in black liquor in small quantities. Those monomers are quantitatively converted, as they are not present in any of the product samples after 12 hours. Combined with the GPC-based information about the removal of monomeric and small oligomeric compounds, we can conclude that the main mechanism of lignin conversion is 1. oxidative activation and 2. condensation to compounds that are larger than the feedstock. The phenolics present in black liquor are consumed during the condensation, similar to capping agents; however, they end up as parts of the polymeric structure. The increase of the molecular weight in combination with the reduction of the water content by electrolysis and evaporation significantly increases the BL viscosity [7]. Condensation reactions are equilibrium-limited, which is determined by the ratio between water and hydroxyl groups on the one side and ether bonds on the other side. The high lignin: water ratio seems to shift this equilibrium towards further condensation. The removal of water by 1. electrolysis and 2. by the sweep gas flow further increases this ratio favouring further

condensation. In addition, if polymers form deposits or dispersed particles, they took out of this equilibrium shifting towards condensation.
This can be avoided by using capping agents including ethanol, and monomeric lignin compounds in higher concentrations, which can react with the activated carbon groups and terminate the chain reaction [28]. Other works focus on the protection of aryl-OH groups from reactions with activated carbons or formed radicals [14]. This seems effective in selectively producing monomers but introduces additional costs to an industrial process.
For Ni/Ni and Ni/Cu, small amounts of alkyl methyl esters are detected. Their origin is currently under investigation.

4.5 Additional experiments for process understanding

To further pinpoint the cause of certain electrode performance observations, short test campaigns have been performed. Figure 34 shows an experiment applying Ni/SS for six hours at a voltage of 2.0 V. After 3 hours the BL was entirely exchanged, and the experiment was continued. The idea of this experiment was to identify the cause of 1) the foaming during the first 30 minutes and 2) the cause of the current drop over time. Concerning the foaming, as shown in Figure 30, after replacing the BL no foaming was observed. This means this phenomenon should be related to the initial activation/stabilisation of the anode surface.
Regarding the current drop over time, a replacement of partly converted/consumed BL by fresh feedstock does not increase the current to the initial values but rather follows the curve. This indicates that the current drop is related to a slow electrode degradation by oxidation and/or deposit formation.

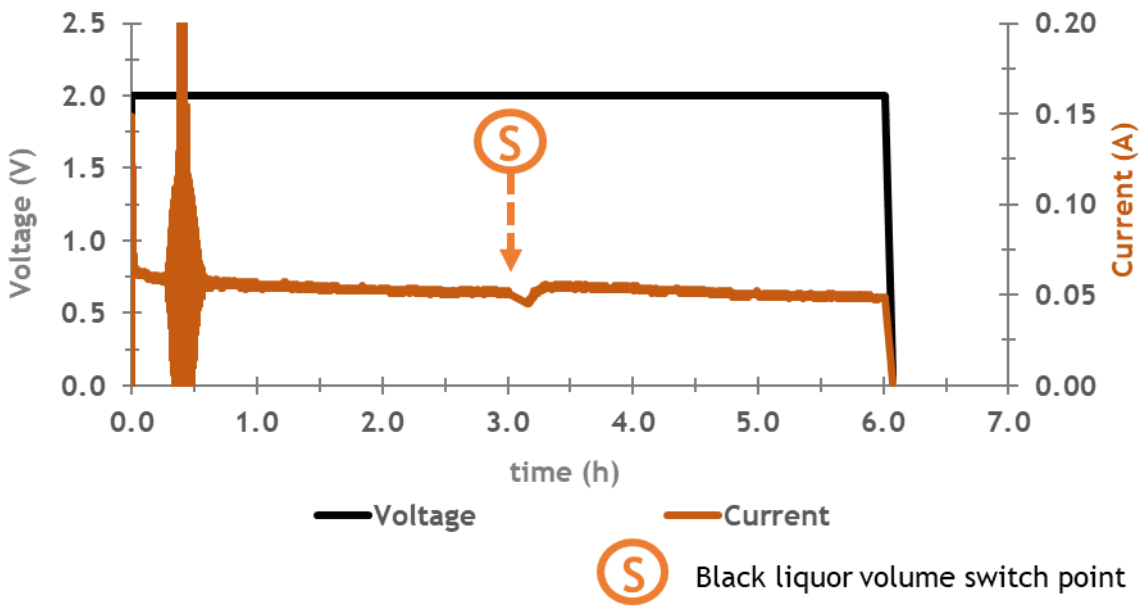

Figure 34 - Effect of fresh volume of BL in the current behaviour.

For the preparation of further studies, the effect of black liquor dilution was tested. Figure 35 shows the current in an electrochemical conversion test with distillate water-diluted BL at 2.0 Volts for 12 hours. As compared to the undiluted black liquor, shown in Figure 28, the initial current is reduced to half, which can be explained by the reduction of the electrolyte conductivity.

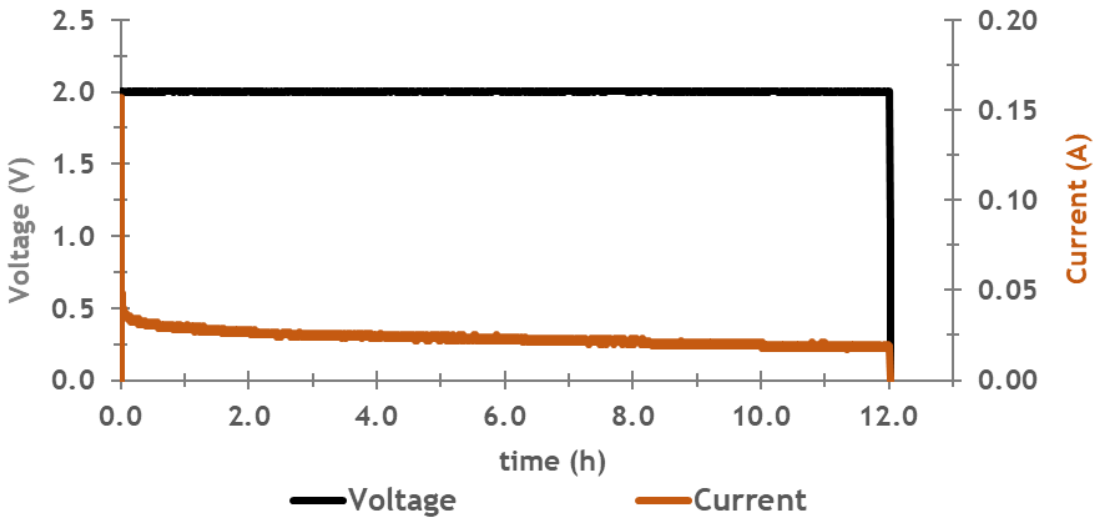

Figure 35 – Ni/Stainless Steel test with diluted BL at 2.0 Volts during twelve hours.

Those values are still high enough for an industrial operation and above the targets of the EBIO project. Further, no initial foaming was observed, which would simplify the industrial start-up. Quantification of gas products was challenging due to the low concentrations of hydrogen. Currently, we adopt the GC method to enable the detection of lower hydrogen levels. The effect of dilution requires an entirely new test campaign, which should include weak black liquor as feedstock. This requires further study of temperature effects, as the operational temperatures of weak and intermediate black liquor are significantly different.

5 Conclusion and recommendations

Within this work, a lab-scale electrochemical setup for black liquor conversion tests has been successfully established and validated. The setup is flexible to operational modes (batch, continuous) and enables online gas product analysis and sampling for offline liquid analysis. Test campaigns studying the effect of electrode material, black liquor dilution rate, and circulation pump flow rate have led to a good understanding of the dominant process parameters. The following conclusions have been established:

Setup design:

- In the current configuration, the reaction is at least partly liquid-solid mass transfer limited by the lignin transport to and polymeric product transport from the electrode surface. This enables running the process in a mass transport limited regime, limiting the lignin transport to the electrode surface. However, using rather concentrated intermediate black lignin, low circulation rates result in the rapid formation of deposits.
- The system should be built more compactly to minimise heat losses in the tubings. Currently, a heating bath temperature of 90 °C results in a cell temperature of 65 °C. This is not critical but limits the operational range towards higher temperatures.
- The loss of water by evaporation into the sweep gas should be minimised to reduce changes in the black liquor viscosity and composition causing deposit formation. The system needs to be operated on an open configuration to prevent pressure build up by produced gas products. Currently, a condenser is designed that will trap and transport most of the water back into the reservoir bottle.

Feedstock:

- Using intermediate black liquor, lignin condensation to larger polymeric fractions seems to be the dominant process. Significant amounts of monomeric phenolics could act as a capping agent. However, the low concentration of monomers present in intermediate black liquor does seem to have only a minor effect. Weak black liquor should be studied instead. The lower lignin/water ratio should significantly improve the process in terms of reaction rates for condensation vs hydrolysis and reduce repolymerisation and deposit formation. The higher anode surface coverage of oxygen can still increase oxygen evolution.

- Higher water concentrations seem to be preferred with respect to lignin depolymerisation and electrode stability.
- The effect of capping agents to suppress lignin condensation should be tested. Though their feasible use in an industrial operation is questionable, their study can give valuable information about the reaction mechanisms and can lead to alternatives not foreseen at this stage.

Process conditions:

- Lower voltages and short residence times should be tested to study the observations of low hydrogen production using Ni/Cu and Ni/Ni electrode combinations. The reduced current can be compensated by increased electrode surface areas by using metal foams, for instance.
- The effect of temperature on the activation and condensation rates needs to be investigated. Preliminary studies have revealed that the current increases with the temperature. A temperature range between 90 and 110 °C is most relevant as it is the temperature most kraft mill evaporation processes operate. Anode overoxidation becomes an issue at temperatures above 120 °C.
- Alternative cell operation should be tested, including divided cells. Physical barriers, such as sinters would enable a consecutive operation of anodic oxidation and cathodic reduction without sacrificing the current densities as in the case of using membranes. Detailed studies of the half reactions using reference electrodes are required.

6 Assessment of the work

6.1 Objectives Achieved

- Overview of the lignocellulosic biomass techniques for fraction of lignocellulosic biomass.
- Overview of the kraft pulping process, understanding the composition of black liquor, kraft lignin structure and current and potential applications.
- Overview of today´s valorisation techniques of black liquor, with a special focus on kraft lignin.
- Electrodes preparation and optimization, Ni/SS, Ni/Ni and Ni/Cu.
- Understanding of electrochemical cell design, assembly and optimization to minimize liquid leaking and simplify product analysis.
- Electrochemical depolymerisation setup establishment, operation, and optimization in terms of gas and liquid phase streams, connection to online gas analysis using the GC and offline liquid sample analysis using SEC, NMR and GCxGC-MS/FID system.
- Study of the experimental conditions of the electrochemical lignin conversion process.
- Understanding, planning and conduction of chronoamperometry step tests and constant voltage stability tests performed using the Ni/SS, Ni/Ni and Ni/Cu electrode combinations.
- Planning and conducting additional experiments for a detailed understanding of specific phenomena encountered during earlier tests.
- Suggestions for scale up to small pilot/bench scale and provisions of operational parameters for process design, in terms of setup design, feedstock and process conditions.
- Recommendations for improvement of lignin conversion and optimisation of the test setup.

6.2 Final assessment

The work performed during this internship demonstrates that the lignin electrochemical conversion process, proposed by the H2020-EBIO project can be a path for the valorisation of the black liquor, with added value for the kraft pulp industry and with benefits for society in terms of sustainable development and the circular economy. At the same time, the work has identified limitations of this approach, specifically concerning the high lignin concentrations in the intermediate black liquor used. Lignin condensation and deposit formation at the electrode surface have been found severe, making the process in its current stage not feasible for scale-up and industrial implementation. For future studies, significantly more diluted black liquors need to be tested. The effect of temperature and electrode surface area needs to be investigated. Other means of minimising condensation reactions should be explored, including the use of capping agents or the separation of intermediates during electrochemical conversion.

7 References

1. Abdelaziz, Omar Y., Clemmensen, Ida, Meier, Sebastian, Costa, Carina A. E., Rodrigues, Alírio E., Hulteberg, Christian P., and Riisager, Anders, *On the Oxidative Valorization of Lignin to High-Value Chemicals: A Critical Review of Opportunities and Challenges*. ChemSusChem, 2022. **15**(20): p. e202201232.
2. Araújo, José Daniel Pacheco, *Production of vanillin from lignin present in the kraft black liquor of the pulp and paper industry*, in *Biological and Chemical Engineering*. 2008, Faculty of Engineering of University of Porto: Porto. p. 1-372.
3. Bajpai, Pratima, *Chapter 2 - Properties, Composition, and Analysis of Black Liquor*, in *Pulp and Paper Industry*, Bajpai, Pratima, Editor. 2017, Elsevier. p. 25-38.
4. Bajwa, D. S., Pourhashem, G., Ullah, A. H. and Bajwa, S. G., *A concise review of current lignin production, applications, products and their environmental impact*. Industrial Crops and Products, 2019. **139**: p. 111526.
5. de Saint Laumer, J. Y., Cicchetti, E., Merle, P., Egger, J. and Chaintreau, A., *Quantification in Gas Chromatography: Prediction of Flame Ionization Detector Response Factors from Combustion Enthalpies and Molecular Structures*. Anal Chem, 2010. **82**(15): p. 6457-6462.
6. Du, Xu, Zhang, Haichuan, Sullivan, Kevin P., Gogoi, Parikshit and Deng, Yulin, *Electrochemical Lignin Conversion*. ChemSusChem, 2020. **Volume XXIII**: p. 4318-4343.
7. EUCALIVA, *EUCAlyptus LIgnin VAlorisation for Advanced Materials and Carbon Fibres*, SL, CONTACTICA, Editor. 2021, European Union Commission: Spain.
8. Figueiredo, Patrícia, Lintinen, Kalle, Hirvonen, Jouni T., Kostiainen, Mauri A. and Santos, Hélder A., *Properties and chemical modifications of lignin: Towards lignin-based nanomaterials for biomedical applications*. Progress in Materials Science, 2018. **93**: p. 233-269.
9. Francisco G. Calvo-Flores, José A. Dobado, Joaquín Isac-García, Francisco J. Martín-Martínez, *Lignin and Lignans as Renewable Raw Materials: Chemistry, Technology and Applications*. Wood Modification–Chemical, Thermal and Other Processes, ed. Christian V. Stevens–Faculty of Bioscience Engineering, Ghent University, Ghent, Belgium. 2015: John Wiley & Sons, Ltd.

10. Garedew, Mahlet, Lam, Chun Ho, Petitjean, Laurene, Huang, Shuquan, Song, Bing, Lin, Fang, . . . Anastas, Paul T., *Electrochemical upgrading of depolymerized lignin: a review of model compound studies*. Green Chemistry, 2021. **23**(8): p. 2868-2899.
11. Ioannis Dogaris, Gunnar Henriksson and Mikael Lindström, *Tall Oil Solubility in Industrial Liquors*, in *Talloljans löslighet i industrilutar*. 2019, Energiforsk p. 1- 72.
12. J. J. Bozell, J. E. Holladay, D. Johnson, and J. F. White *Top Value-Added Chemicals from Biomass*, in *Results of Screening for Potential Candidates from Biorefinery Lignin* 2007, Pacific Northwest National Laboratory, University of Tennessee, National Renewable Energy Laboratory. p. 87.
13. Jeremias, Maria João Ferreira, *Electrochemical valorisation of Kraft black liquor, Optimisation of an electrolyser for obtaining lignin*. 2022, Instituto Superior Técnico, Universidade de Lisboa, Portugal: Lisboa. p. 7.
14. Kim, Kwang Ho and Kim, Chang Soo, *Recent Efforts to Prevent Undesirable Reactions From Fractionation to Depolymerization of Lignin: Toward Maximizing the Value From Lignin*. Frontiers in Energy Research, 2018. **6**.
15. Lange, Heiko, Decina, Silvia and Crestini, Claudia, *Oxidative upgrade of lignin – Recent routes reviewed*. European Polymer Journal, 2013. **49**: p. 1151–1173.
16. Li, P., Ren, J., Jiang, Z., Huang, L., Wu, C., and Wu, W., *Review on the preparation of fuels and chemicals based on lignin*. RSC Adv, 2022. **12**(17): p. 10289-10305.
17. Morgana, Massimo, Viola, Egidio, Francesco, Zimbardi Nadia, Cerone, Assunta, Romanelli and Vito, Valerio, *Depolymerization and Hydrogenation of Organosolv Eucalyptus Lignin by Using Nickel Raney Catalyst*. Processes 2021. **Volume IX**: p. 1-18.
18. Mussatto, S. I. and Dragone, G. M., *Chapter 1 - Biomass Pretreatment, Biorefineries, and Potential Products for a Bioeconomy Development*, in *Biomass Fractionation Technologies for a Lignocellulosic Feedstock Based Biorefinery*, Mussatto, Solange I., Editor. 2016, Elsevier: Amsterdam. p. 1-22.
19. Nadányi, Richard, Ház, Aleš, Lisý, Anton, Jablonský, Michal, Šurina, Igor, Majová, Veronika, and Baco, Andrej, *Lignin Modifications, Applications, and Possible Market Prices*. Energies, 2022. **15**(18): p. 6520.
20. Nidhi Sharma, Bhawana, R. D. Godiyal,B. P. Thapliyal4, *A Review on Pulping, Bleaching and Papermaking Processes*. Journal of Graphic Era University 2020. **Volume VIII**: p. 1-18.

21. Oliveira, R. C. P., Mateus, M. M. and Santos, D. M. F., *Editors' Choice—On the Oxidation of Kraft Black Liquor for Lignin Recovery: A Voltammetric Study*. Journal of The Electrochemical Society, 2019. **166**(16): p. E547.
22. Oliveira, R. C. P., Mateus, M. and Santos, D. M. F., *Chronoamperometric and chronopotentiometric investigation of Kraft black liquor*. International Journal of Hydrogen Energy, 2018. **43**(35): p. 16817-16823.
23. Paula, Sara Cristina da Silva, *Precipitation of lignin from kraft black liquor*, in *Departamento de Engenharia Química*. 2010, FEUP: Porto.
24. R. Oliveira, M. Mateus, D.M.F. Santos, *First insights on the electrochemical valorisation of black liquor*, 2022; Disponível em: https://fenix.tecnico.ulisboa.pt/downloadFile/563345090414664/Resumo%20Alargado%20-%20Raisa%20Oliveira,%20n%2069337.pdf.
25. Rößiger, Björn, Unkelbach, Gerd and Pufky-Heinrich, Daniela, *Base-Catalyzed Depolymerization of Lignin: History, Challenges and Perspectives*. 2018.
26. Roy, Ranen, Rahman, Md Sajjadur, Amit, Tanvir A. and Jadhav, Balawanthrao, *Recent Advances in Lignin Depolymerization Techniques: A Comparative Overview of Traditional and Greener Approaches*. Biomass, 2022. **Volume II**: p. 130-154.
27. Tran, Honghi and Vakkilainen, Esa, *THE KRAFT CHEMCIAL RECOVERY PROCESS*. 2016. **Volume I**: p. 1-8.
28. Wei, Ni, Qi, Shuang, Wang, Guanhua, Ge, Jing, Sui, Wenjie, Sun, Hao, . . . Si, Chuanling, *Acid-promoted lignin reductive depolymerization under mild conditions via a condensation minimizing approach: From organosolv lignin to woody biomass*. Fuel, 2023. **338**: p. 127311.

Appendix A – Material and Methods

A.1 Liquid Phase Equipment's

This section presents the data obtained for the calibration of the Black liquor circulation rate, Table 6, Table 7 and Table 8, representing the circulation flow rate measurements as a function of the pump speed voltage.

Table 6 - BL circulation flow rate at 20 Volts pump speed.

	Time (s)	Volume (mL)	Pump Voltage Speed	Weight (g)
1	20.0	40.0	20.0	53.0
2	20.6	40.0	20.0	51.0
3	28.6	40.0	20.0	51.0
Average:	24.6	---	---	5.7
Circulation flow rate Rate black liquor (g/s):				2.10

Table 7 - BL circulation flow rate rate at 15 Volts pump speed.

	Time (s)	Volume (mL)	Pump Voltage Speed	Weight (g)
1	24.0	40.0	15.0	50.0
2	24.5	40.0	15.0	51.0
3	27.1	40.0	15.0	51.0
Average:	25.2	---	---	50.7
Circulation flow rate Rate black liquor (g/s):				2.01

Table 8- BL circulation flow rate at 10 Volts pump speed.

	Time (s)	Volume (mL)	Pump Voltage Speed	Weight (g)
1	53.3	40.0	10.0	40.0
2	57.6	40.0	10.0	46.0
3	50.0	40.0	10.0	46.0
Average:	53.6	---	---	46.0
Circulation flow rate Rate black liquor (g/s):				0.82

A.2 Gas Phase Equipment´s

This section presents the data used to perform the calibration of the carrier gas within the mass flow controller associated and the GC calibration for four different feed gas. Table 9, Table 11, Table 12 and Table 13 show the gas mass flow controller calibration data referent to the time necessary to fill up the column of the bubble gas flow meter with seven millilitres of soap as a function of the gas flow rate percentage out of full mass flow controller scale.

Table 9 – Time(s) obtained to calculate the flow of the carrier gas passing through the mass flow controller at 2.0 %.

With 2.0 N2%	**@**	**T**	24.00	**ºC**
	@	**P**	1024.30	**hPa**
	@	**Volume**	7.00	**mL**
	time(s)	**Vflow (mL/s)**	**Vflow (mL/min)**	**Average (mL/min)**
1	58.73	0.12	7.15	7.25
2	58.28	0.12	7.21	
3	58.22	0.12	7.21	
4	57.59	0.12	7.29	
5	56.84	0.12	7.39	
6	57.53	0.12	7.30	7.35
7	57.48	0.12	7.31	
8	56.94	0.12	7.38	
9	57.36	0.12	7.32	
10	56.29	0.12	7.46	

Table 10 – Time (s) obtained to calculate the flow of the carrier gas passing through the mass flow controller at 5.3 %.

With 5.3 N2%	@	T	24.00	°C
	@	P	1024.30	hPa
	@	Volume	7.00	mL
	time(s)	Vflow (mL/s)	Vflow (mL/min)	Average (mL/min)
1	21.23	0.33	19.78	20.39
2	20.93	0.33	20.07	
3	20.71	0.34	20.28	
4	20.16	0.35	20.83	
5	19.99	0.35	21.01	
6	19.73	0.35	21.29	20.63
7	19.80	0.35	21.21	
8	20.77	0.34	20.22	
9	20.73	0.34	20.26	
10	20.83	0.34	20.16	

Table 11 - Time(s) obtained to calculate the flow of the carrier gas passing through the mass flow controller at 6.5 %.

With 6.5 N2%	@	T	24.00	°C
	@	P	1024.30	hPa
	@	Volume	7.00	mL
	time(s)	Vflow (mL/s)	Vflow (mL/min)	Average (mL/min)
1	16.91	0.41	24.84	25.15
2	16.93	0.41	24.81	
3	16.68	0.42	25.18	
4	16.54	0.42	25.39	
5	16.46	0.43	25.52	
6	16.63	0.42	25.26	25.75
7	16.16	0.43	25.99	
8	16.00	0.44	26.25	
9	16.56	0.42	25.36	
10	16.23	0.43	25.88	

Table 12 - Time(s) obtained to calculate the flow of the carrier gas passing through the mass flow controller at 8.0 %.

With 8.0 N2%	@	T	24.00	ºC
	@	P	1024.30	hPa
	@	Volume	7.00	mL
	time(s)	Vflow (mL/s)	Vflow (mL/min)	Average (mL/min)
1	12.38	0.57	33.93	31.02
2	15.18	0.46	27.67	
3	13.58	0.52	30.93	
4	13.46	0.52	31.20	
5	13.38	0.52	31.39	
6	13.36	0.52	31.44	31.60
7	13.14	0.53	31.96	
8	13.19	0.53	31.84	
9	13.36	0.52	31.44	
10	13.40	0.52	31.34	

Table 13 - Time(s) obtained to calculate the flow of the carrier gas passing through the mass flow controller at 10.0 %.

With 10.0 N2%	@	T	24.00	ºC
	@	P	1024.30	hPa
	@	Volume	7.00	mL
	time(s)	Vflow (mL/s)	Vflow (mL/min)	Average (mL/min)
1	10.51	0.67	39.96	40.06
2	10.51	0.67	39.96	
3	10.37	0.68	40.50	
4	10.42	0.67	40.31	
5	10.61	0.66	39.59	
6	10.41	0.67	40.35	39.90
7	10.57	0.66	39.74	
8	10.46	0.67	40.15	
9	10.62	0.66	39.55	
10	10.57	0.66	39.74	

Table 14, Table 15, Table 16 and Table 17 show the percentage (V/V) of each gas present in bottle A, B, C, D used to obtain the peak areas, Table 18, after being injected and analysed by the GC.

Table 14 - Bottle gas A, composition and concentration and respective peak area measured by GC analysis.

Bootle A		
Gas name	**Concentration % (V/V)**	**Peak (a.u)**
H_2	59.60	5108533
CO_2	15.20	65223654
N_2	17.33	56975984
CH_4	0.61	1636931
CO_2	6.06	22760879
O_2	---	---

Table 15 - Bottle gas B, composition and concentration and respective peak area measured by GC analysis.

Gas name	Concentration % (V/V)	Peak (a.u)
N_2	78.00	108485551
O_2	21.00	78322396
H_2	---	---
---	---	---
---	---	---
---	---	---

Table 16 - Bottle gas C, composition and concentration and respective peak area measured by GC analysis.

Gas name	Concentration % (V/V)	Peak (a.u)
CH_3OH	1.00	1844725
CO	2.04	6692971
CO_2	2.02	6425920
H_2	10.10	488430
N_2	84.84	113478752
O_2	---	---

Table 17 – Bottle gas D, composition and concentration and respective peak area measured by GC analysis.

Gas name	Concentration % (V/V)	Peak (a.u)
CO_2	8.04	26868661
CH_4	14.10	34334726
CO	1.00	3399087
N_2	14.10	41104425
H_2	62.76	4727125
O_2	---	---

Table 18 - Hydrogen and Oxygen gas ratio and concentration ratio.

Gas Bottle	Peak Ratio		Concentration Ratio	
	AH2/AN2	AO2/AN2	CH2/CN2	CO2/CN2
Bootle A	0.09	0.00	3.44	0.00
Bootle B	0.00	0.72	0.00	0.27
Bootle C	0.00	0.00	0.12	0.00
Bootle D	0.12	0.00	4.45	0.00

Appendix B – Results and Discussion

B.1 H-NMR Results

C^{13}-NMR Results:

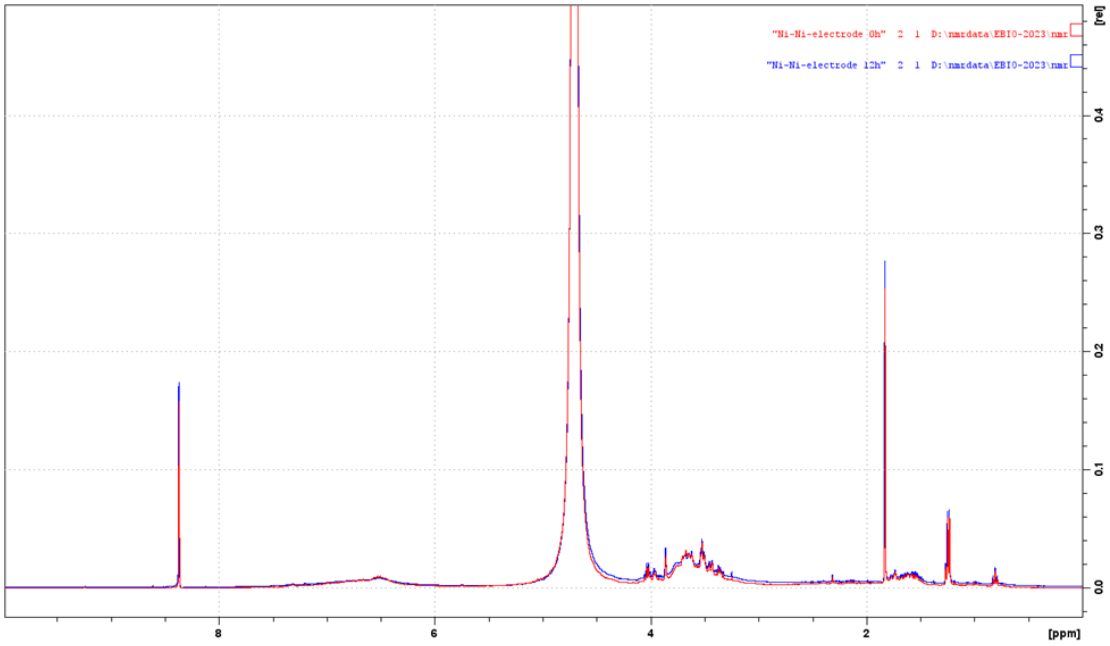

Figure 36 - H-NMR of liquid sample, Ni/Ni-electrode, 0 hours (red) and sample Ni/Ni- electrode 12 hours.

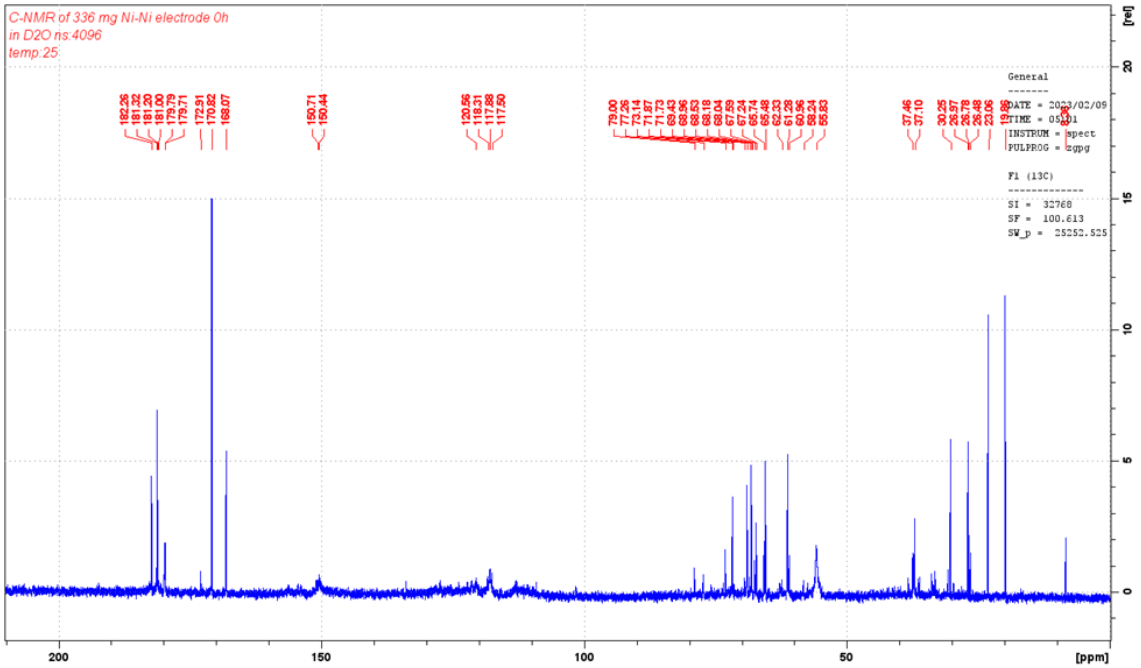

Figure 37 - C-NMR of 336 mg Ni/Ni-electrode 0 hours.

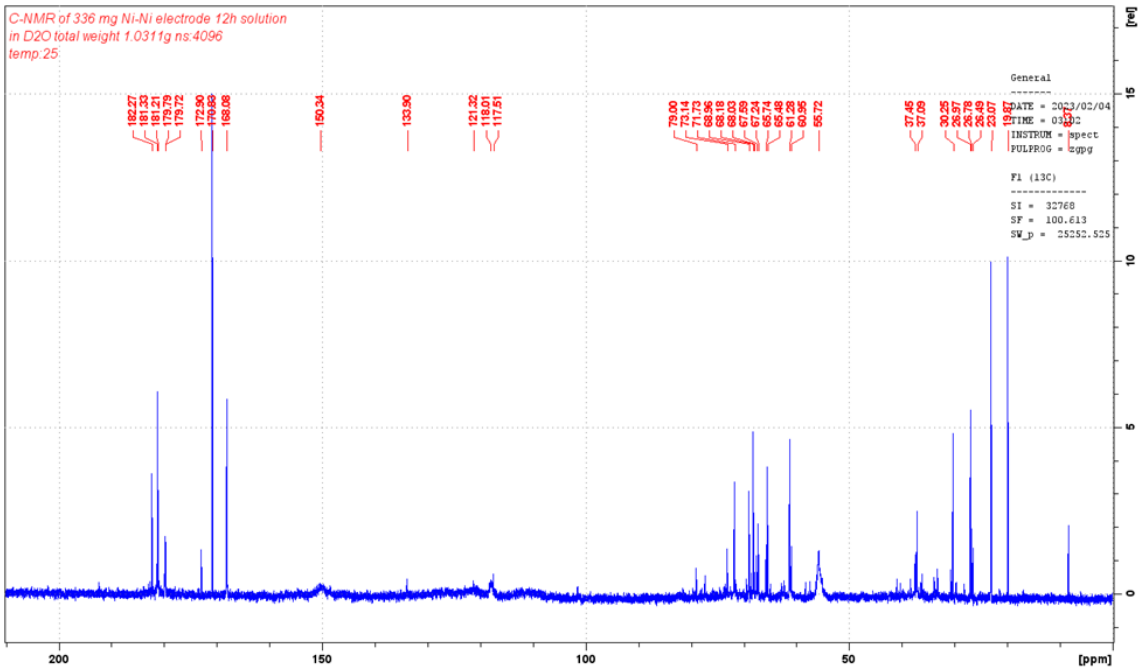

Figure 38 - C-NMR of 336 mg Ni/Ni-electrode 12 hours.

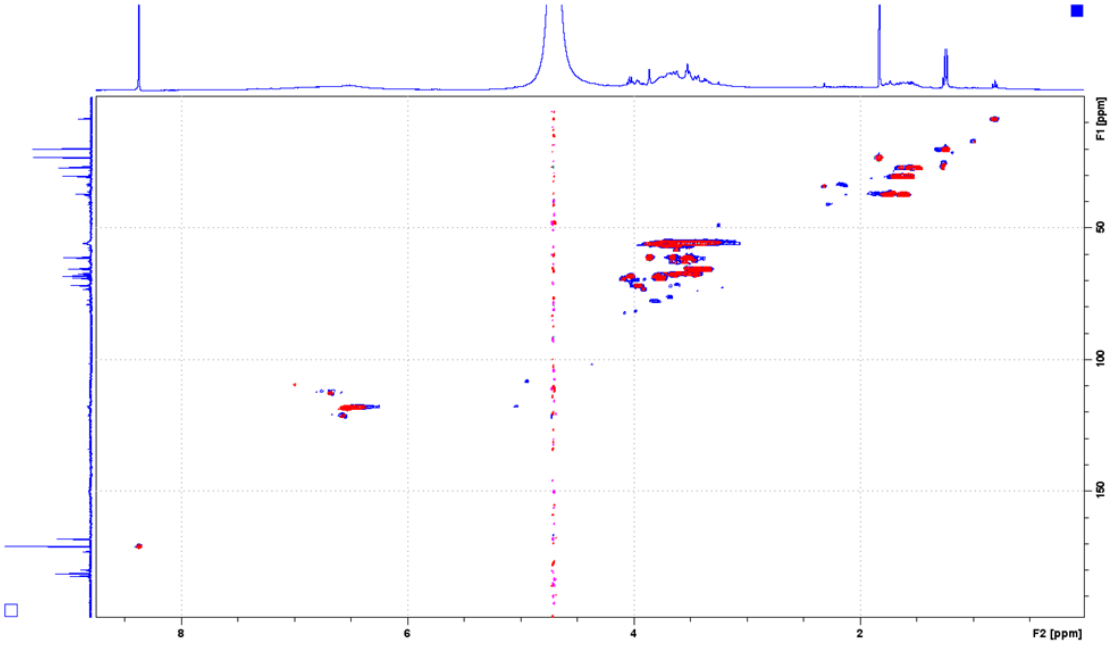

Figure 39 – Heteronuclear single quantum coherence spectrum: Red: Ni/Ni- electrode 0 hours; Blue: Ni/Ni- electrode 12 hours.